Glacial history of the Åsgardfonna Ice Cap, NE Spitsbergen, since the last glaciation

Lis Allaart [a, b, *], Anders Schomacker [a], Nicolaj K. Larsen [c], Egon Nørmark [d], Tom Arne Rydningen [a], Wesley R. Farnsworth [e], Michael Retelle [b, f], Skafti Brynjólfsson [g], Matthias Forwick [a], Sofia E. Kjellman [a]

[a] Department of Geosciences, UiT the Arctic University of Norway, Postboks 6050 Langnes, Tromsø, N-9037, Norway
[b] Department of Arctic Geology, The University Centre in Svalbard (UNIS), P.O. Box 156, Longyearbyen, N-9171, Norway
[c] GLOBE Institute, Section for GeoGenetics, University of Copenhagen, Øster Voldgade 5-7, Copenhagen K., DK-1350, Denmark
[d] Department of Geoscience, Aarhus University, Høegh-Guldbergs Gade 2, Aarhus C., DK-8000, Denmark
[e] Nordic Volcanological Center, Institute of Earth Sciences, University of Iceland, Askja, Sturlugata 7, Reykjavík, IS-101, Iceland
[f] Bates College, Department of Earth and Climate Sciences, Lewiston ME, 04240, Maine, USA
[g] The Icelandic Institute of Natural History, Borgum við Norðurslóð, IS-600, Akureyri, Iceland

ARTICLE INFO

ABSTRACT

The response of glaciers and ice caps to past climate change provides important insight into how they will react to ongoing and future global warming. In Svalbard, the Holocene glacial history has been studied for many cirque and valley glaciers. However, little is known about how the larger ice caps in Svalbard responded to Late Glacial and Holocene climate changes. Here we use lake sediment cores and geophysical data from Femmilsjøen, one of Svalbard's largest lakes, to reconstruct the glacial history of the Åsgardfonna Ice Cap since the last deglaciation. We find that Femmilsjøen potentially deglaciated prior to 16.1 ± 0.3 cal ka BP and became isolated from the marine environment between 11.7 ± 0.3 to 11.3 ± 0.2 cal ka BP. Glacial meltwater runoff was absent between 10.1 ± 0.4 and 3.2 ± 0.2 cal ka BP, indicating that Åsgardfonna was greatly reduced or disappeared in the Early and Middle Holocene. Deposition of glacial-meltwater sediments re-commenced in Femmilsjøen at c. 3.2 ± 0.2 cal ka BP, indicating glacier re-growth in the Femmilsjøen catchment and the onset of the Neoglacial. The glacier(s) in the Femmilsjøen catchment area reached sizes no smaller than their modern extents already at c. 2.1 ± 0.7 cal ka BP. Our results suggest that larger Svalbard ice caps such as Åsgardfonna are very sensitive to climate changes and probably melted completely during the Holocene Thermal Maximum. Such information can be used as important constraints in future ice-cap simulations.

© 2020 The Author(s). Published by Elsevier Ltd. This is an open access article under the CC BY license (http://creativecommons.org/licenses/by/4.0/).

1. Introduction

Understanding how the glaciers and ice caps in Svalbard responded to climate variability during the Late Glacial and Holocene may provide important information about how they will react to ongoing and future global warming (Forwick and Vorren, 2009; Miller et al., 2017; Bakke et al., 2018). Through the Holocene, the major driver of climate change has been insolation (Briner et al., 2016). The orbital forcing in the Early Holocene led to peak summer insolation in the northern hemisphere between c. 12.0 and 11.0 cal ka BP providing warm climate boundary conditions, however, still with strong seasonal variability (Berger, 1978; Bradley et al., 2003; Laskar et al., 2004). The glacial response to the warm Early Holocene climate could be regarded an analogue for how glaciers and ice caps might act in a warmer climate in the future. Svalbard is an ideal location for studying the impact and interaction of orbital, atmospheric and oceanic forcings on glaciers and climate. The climate of the archipelago is strongly coupled to the heat advection from the West Spitsbergen Current (Fig. 1), and it is very sensitive to even small changes in the configuration of the water and air masses surrounding Svalbard (Aagaard et al., 1987; Rasmussen et al., 2013; Bakke et al., 2018; Hanssen-Bauer et al., 2019).

* Corresponding author. Department of Geosciences, UiT the Arctic University of Norway, Postboks 6050 Langnes, N-9037, Tromsø, Norway.
E-mail address: lis.allaart@uit.no (L. Allaart).

Fig. 1. (a) Overview map of Svalbard. All place names mentioned in text are marked with a black dot and a name label. The study area of Femmilsjøen is marked with a red dot. Map based on Digital Elevation Model (DEM) of Svalbard and TopoSvalbard shapefiles, © Norwegian Polar Institute, 2019. (b) Inset map showing the location of Svalbard in the Arctic region, warm currents in red (NAC = North Atlantic Current, NCC = North Cape Current and WSC = West Spitsbergen Current) and cold currents in blue (ESC = East Spitsbergen Current, EGC = East Greenland Current). (For interpretation of the references to colour in this figure legend, the reader is referred to the Web version of this article.)

To improve regional climate reconstructions and forecast scenarios in Svalbard, local climate archives should be included in the numerical models. The Svalbard ice-core records only cover the past *c.* 1.0 ka (Isaksson et al., 2005; Kekonen et al., 2005; Divine et al., 2011) and therefore, there is a need for data series from high-resolution marine and lacustrine sedimentary records. Such records extend further back in time than the ice cores, and when integrated in regional climate models, they may improve the understanding of how glaciers in the high Arctic respond to present and future warming (Bakke et al., 2018; Fischer et al., 2018; van der Bilt et al., 2019).

Marine, terrestrial, and lacustrine geological records sometimes lag each other, challenging detailed reconstructions of the Holocene climatic and glacial events (e.g., Forwick and Vorren, 2009; Farnsworth et al., 2017; Bakke et al., 2018). However, the last

deglaciation across the Svalbard archipelago and the approximate onset of the HTM are relatively well constrained (e.g., Svendsen et al., 1992; Landvik et al., 2003; Hald et al., 2004; Hormes et al., 2013; Rasmussen et al., 2013; Hogan et al., 2017). Lake sediment records have been used widely to reconstruct the Holocene ice and climate history of Svalbard (e.g., Svendsen et al., 1987; Birks, 1991; Snyder et al., 1994; Svendsen and Mangerud, 1997; Mäusbacher et al., 2002; Røthe et al., 2018; Bakke et al., 2018). All of these studies focus on lakes that record changes in cirque glaciers or on reconstructing past temperatures. However, there is still a need for investigations of continuous climate archives that record changes of the larger ice caps on Svalbard in order to decipher whether the ice caps survived the HTM, to identify the timing of the Holocene glacier minima, and to reconstruct the timing of the onset of the Neoglacial (Schomacker et al., 2019).
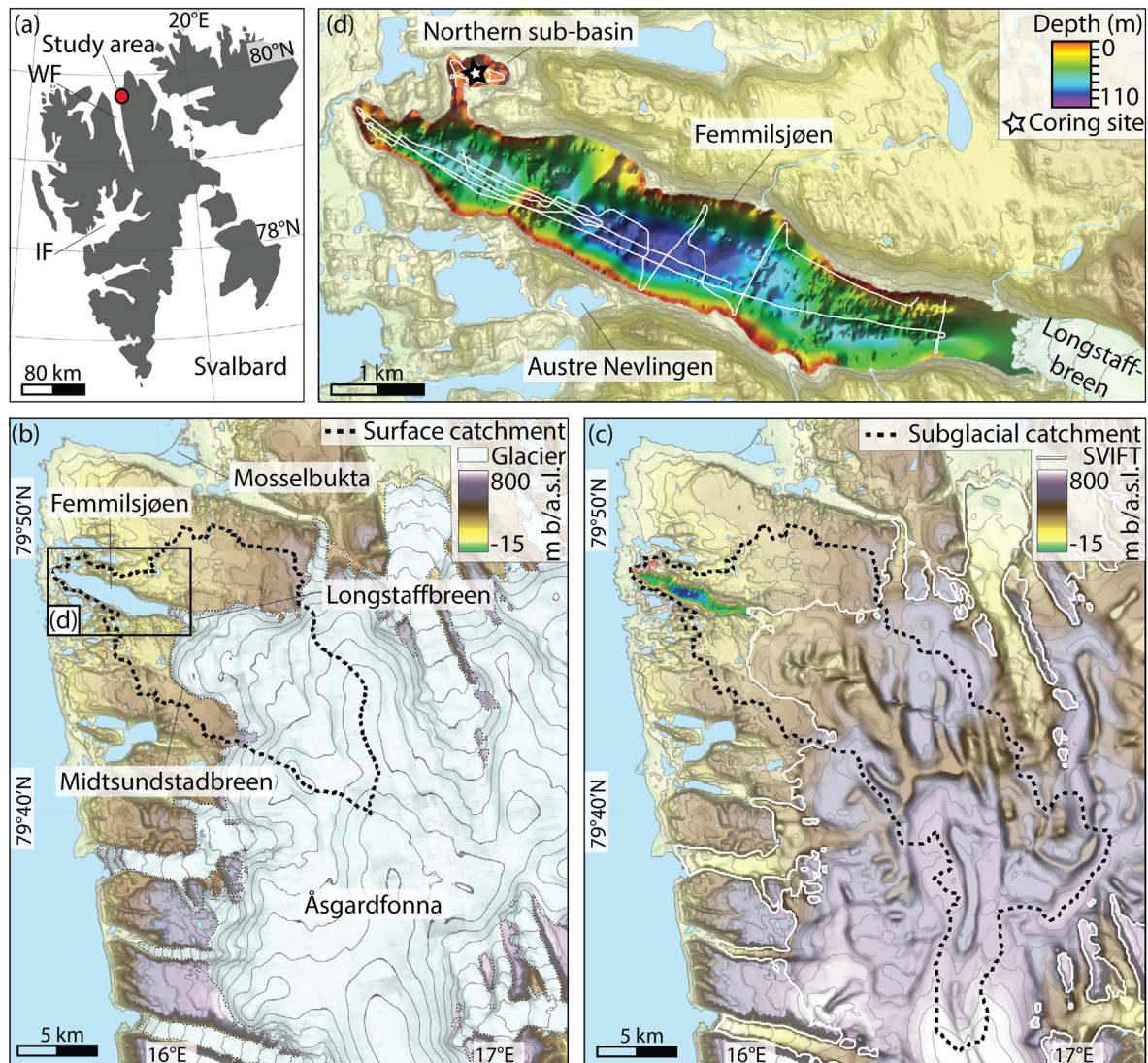
Fig. 2. (a) Overview map of Svalbard, location of the study area. The location of Wijdefjorden (WF) and Isfjorden (IF) are marked. (b) DEM of NE Spitsbergen showing the surface catchment area of Femmilsjøen (black, dashed line, calculations based on the DEM from © Norwegian Polar Institute, 2019) and the current glacial extent. (c) Composite DEM of NE Spitsbergen showing the subglacial terrain (white line, based on the SVIFT dataset, Fürst et al., 2018). Subglacial catchment of Femmilsjøen (calculations based on the composite DEM) (black dashed line) and bathymetry of Femmilsjøen are indicated. (d) Detail map of the bathymetry of Femmilsjøen, locations of the collected sub-bottom profiler data (white lines) and coring site (white star).

In this study, we use lake sediment records and geophysical data from Lake Femmilsjøen to reconstruct the glacial history of the NW part of the Åsgardfonna Ice Cap, NE Spitsbergen since the last glaciation (Figs. 1 and 2). Furthermore, we compare the Femmilsjøen record to a marine record from northern Wijdefjorden (Allaart et al., 2020) and discuss similarities and differences in the climatic development archived in the marine and terrestrial records. Finally, we place our findings in a Circum-Arctic perspective.

2. Setting

2.1. Glacial history

Surface exposure (^{10}Be) ages from NW Spitsbergen suggest that ice sheet thinning had commenced between 25 and 20 ka ago, and that ice had retreated from Woodfjorden between 16 and 14 ka ago, while Reinsdyrflya, a strand flat west of the mouth of Woodfjorden, had become completely ice-free prior to the onset of the Holocene

(Gjermundsen et al., 2013; Fig. 1). Minimum limiting ^{14}C dating of marine sediment cores indicate that the mouths of Woodfjorden and Wijdefjorden deglaciated prior to 15.2 ± 0.5 and 12.0 ± 0.3 cal ka BP, respectively (Fig. 1; Bartels et al., 2017; Allaart et al., 2020), supporting an early deglaciation of northern Spitsbergen. In comparison, the mouth of Isfjorden (in central Spitsbergen) deglaciated *c.* 14.1 cal ka BP (Fig. 1; Mangerud et al., 1992; Forwick and Vorren, 2009). The fjords subsequently experienced episodic glacial retreat and the inner parts of all three fjords (Isfjorden, Woodfjorden and Wijdefjorden) were deglaciated *c.* 11.0 cal ka BP (Baeten et al., 2010; Bartels et al., 2017; Braun, 2019; Allaart et al., 2020). In some areas of Svalbard, dynamic advances of smaller tributary glaciers occurred right after retreat of the main valley glaciers (Lønne et al., 2005; Larsen et al., 2018; Farnsworth et al., 2017, 2018). Sedimentary ancient DNA (*sed*aDNA) from a lake record from Jodavannet (in central Wijdefjorden, Fig. 1) reveals a rapid colonization after glacial retreat, with establishment of half of the Holocene plant taxa prior to 10.6 cal ka BP (Voldstad et al., 2020).

The HTM is generally recognised earlier in the marine environment (*c.* 11.2−7.7 cal ka BP) than in the terrestrial and lacustrine (*c.* 10.5−7.8 cal ka BP) environments (e.g., Salvigsen et al., 1992; Hald et al., 2004; van der Bilt et al., 2015; Bakke et al., 2018; Bartels et al., 2018; Mangerud and Svendsen, 2018). While marine sediment records (e.g., Hald et al., 2004; Forwick and Vorren, 2009; Baeten et al., 2010; Rasmussen et al., 2013) and glacial isostatic adjustment modelling (Fjeldskaar et al., 2018) indicate that some large glaciers and ice caps persisted through the HTM, the timing and ice configuration of the Holocene glacier minimum is not well constrained (Bakke et al., 2018). Furthermore, it remains unknown if the Holocene glacial minimum occurred time-transgressively across the archipelago. Lacustrine archives from the west coast of Spitsbergen indicate that smaller glaciers completely vanished from their lake catchments during the Early and Middle Holocene (Svendsen and Mangerud, 1997; Røthe et al., 2015; de Wet et al., 2017). In contrast, marine records suggest that Spitsbergen's inner fjords never completely deglaciated and tidewater glaciers persisted through the entire Holocene, and thus survived the HTM (Hald et al., 2004; Forwick and Vorren, 2009; Rasmussen et al., 2013; Farnsworth et al., 2020). In Woodfjorden, Wijdefjorden and Wahlenbergfjorden in northern Svalbard (Fig. 1) low sedimentation rates and coincident maximum water temperatures suggest limited glacial activity during the HTM (Flink et al., 2017; Bartels et al., 2018; Allaart et al., 2020). However, coarse-grained debris attributed to ice rafting occur throughout the Wahlenbergfjorden record, indicating the presence of sea ice or glacier ice (Flink et al., 2017; Bartels et al., 2018). Modelling of the Holocene glacial isostatic rebound supports that (smaller) glaciers in western and northern Spitsbergen were absent during the HTM. Lower uplift rates in Nordaustlandet and eastern Spitsbergen suggest that the ice caps in these areas persisted through the HTM (Fjeldskaar et al., 2018).

In the Late Holocene, glaciers grew during the Neoglacial, induced by decreasing Northern Hemisphere summer temperatures (Svendsen and Mangerud, 1997; Hald et al., 2004; Laskar et al., 2004; Forwick and Vorren, 2009; van der Bilt et al., 2015). The onset of Neoglacial expansion is characterised by incremental steps of glacier expansion between 4.5 and 0.5 cal ka BP (Bakke et al., 2018; Bradley and Bakke, 2019). A key remaining question is whether the Little Ice Age (LIA) was a separate cold spell, or if it represents the ultimate Neoglacial glacier advances (Svendsen and Mangerud, 1997; Miller et al., 2017).

2.2. Femmilsjøen

Femmilsjøen (meaning 'the five mile lake' in Norwegian) is a glacier-fed isolation basin located in NE Spitsbergen (Fig. 2). To our knowledge, previous studies of the lake and its water mass structure do not exist; however, it is most likely oligotrophic and cold monomictic (Smith and Ashley, 1985). The lake is ~7.6 km long, up to ~1.3 km wide, has a surface area of 7.6 km^2 and water depths exceed 100 m qualifying Femmilsjøen as one of the largest lakes in Svalbard by both surface area and volume. A sill, 100 m wide and a maximum of 5 m depth, separates a northern sub-basin (0.21 km^2 and 15 m deep) from the main lake basin (Fig. 2). The outlet and marine isolation threshold in the western end of the main lake basin constitutes a ~50 m wide channel (Fig. 3). The current elevation of the threshold is ~26 m a.s.l.

The subaerial and subglacial catchment areas are 173.5 km^2 and 304.4 km^2, respectively (Fig. 2b and c). The border of the subglacial catchment area denotes the threshold for the inflow of glacial meltwater. From here we use 'catchment area' when referring to the full subglacial catchment area. Femmilsjøen receives meltwater from the NW part of the Åsgardfonna Ice Cap (1230 km^2 in 1993; Hagen et al., 1993). Four rivers feed into the lake: two originate
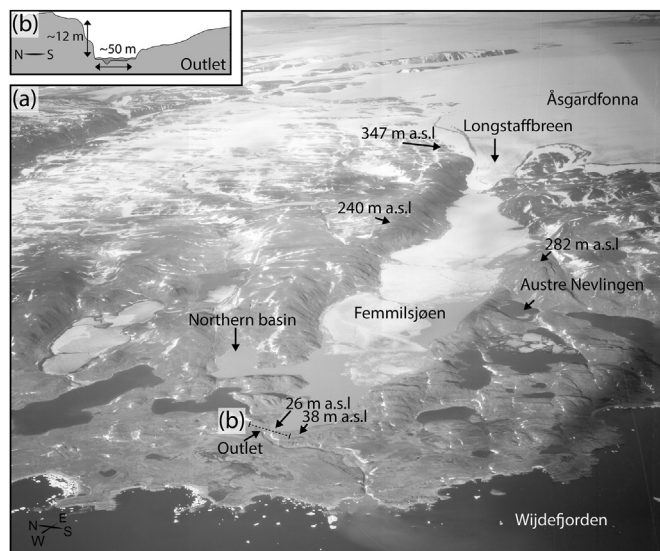

Fig. 3. (a) Oblique aerial image of Femmilsjøen and its surroundings, view approximately towards east (© Norwegian Polar Institute, 1936). The distance of the foreground in this image equals ~4 km at the lower edge, and Femmilsjøen is ~7.6 km long. (b) Cross profile of the outlet and marine isolation threshold of Femmilsjøen (in the western end of the lake).

from lakes located north of, and at higher altitudes than Femmilsjøen and two (south of Femmilsjøen) supply meltwater from Midtsundstadbreen (an outlet of Åsgardfonna) to the lake (Fig. 1d). Small deltas occur where the rivers enter the lake. In its eastern end, Femmilsjøen receives direct runoff from Longstaffbreen (an outlet of Åsgardfonna) and icebergs calve into the lake. Longstaffbreen is a surge-type glacier, with its latest documented active phase in 1960 (Liestøl, 1993; Hagen et al., 1993; Lønne, 2016). The lake water is turbid from sediment in suspension during the ice-free period (estimated to be July to September; Holm et al., 2012), and the water surface across the entire lake is opaque. Most of the surrounding terrain is steep (Fig. 3), except from the area around the westernmost end of the lake, where the outlet towards Wijdefjorden is located (Fig. 2). The postglacial marine limit in Mosselbukta (~10 km north of Femmilsjøen; Figs. 1 and 2b) is 65 m a.s.l. (Salvigsen and Österholm, 1982). Beach ridges and marine sediments observed up to similar elevations during fieldwork and on aerial images indicate a similar marine limit in the Femmilsjøen area.

The bedrock in the catchment area is Precambrian and consists of mica schist, quartzite, amphibolite, granitic/granodioritic gneiss, locally migmatitic, subordinate amphibolite, metadolerite, mica gneiss, garnet-mica schist and phyllite (Dallmann, 2015). Subordinate marble occurs in the Rittervatnet and Polheim units in the central part of the catchment, and greywacke, dolostone and limestone belonging to the Kingbreen Formation in the easternmost part (Dallmann, 2015).

3. Material and methods

3.1. Bathymetry and sub-bottom data

The acoustic survey of the lake was conducted in lines predominantly along and perpendicular to the long axis of the lake with a small fiberglass vessel. Single beam bathymetric data were collected with a Garmin Echomap Plus 73SV with a CV52HW-TM transducer and a 5 Hz receiver, using the Quick Draw contour function. The XYZ-points were exported from the instrument and

imported to Petrel in UTM zone 33 N (datum: WGS84) and gridded in a 5 × 5 m horizontal resolution using the convergent interpolation method. Re-gridding to 10 × 10 m reduced noise in the dataset and gave a smoother appearance. Hence, the 10 × 10 m grid was used as basis for the maps.

Sub-bottom data were collected with a PINGER sub-bottom profiler, with a signal frequency of 3.5 kHz, 1 ping per second and a 3−7 kHz bandwidth. Sampling frequencies ranged between 10 and 18 kHz. The signal was recorded on a Mini Trace System. A total number of 22 lines with a combined length of 43 km were recorded. Bandpass filtering was carried out on all data with a low-cut filter at 1000 Hz and high-cut filter at 6000 Hz. Moreover, amplitude recovery was made in order to compensate for spherical divergence and absorption. Finally, a constant scaling was applied on each trace to achieve uniform trace amplitudes. The data were interpreted in the Kingdom Suite ® 8.8 seismic. A sound velocity of 1500 ms^{-1} was used to calculate depth and thickness (Trottier et al., 2019).

3.2. Sediment cores

Three sediment cores (FMP1, FMP2 and FMP3) were retrieved from the 15 m deep sub-basin in the northern part of Femmilsjøen (79.805308 °N, 15.730763 °E; Fig. 2). Coring was conducted from a small inflatable rubber boat using a hand-held light-weight piston corer with 6 cm diameter coring tubes. Water depths of >100 m prevented coring in the main basin with this type of equipment. The rubber boat was anchored to a stable position and the cores were retrieved through a hole in the floor of the boat. The three sediment cores (98.5, 156.5 and 108 cm long, respectively) were retrieved successively deeper in the sediments and a substantial overlap between each core and the next was secured in order to collect a continuous sediment record. Sediment-water mixing in the lower parts of FMP2 was observed immediately after coring, and therefore, the analyses focus on FMP1 and FMP3. The sediment-water interface was preserved in FMP1.

3.3. Geophysical, geochemical and lithological properties

After splitting, X-radiographs of the sediment core halves were acquired using a Geotek Standard X-ray CT system (XCT). Line-scan images of the sediment surface were acquired with a Jai L-107CC 3 CCD RGB Line Scan Camera mounted on an Avaatech X-ray fluorescence (XRF) core scanner.

The Avaatech XRF core scanner was also used to carry out qualitative measurements of the element-geochemical composition of the sediment surfaces using a Rhodium X-ray source. Prior to the measurements, the sediment surface was smoothened and covered with a 4 μm ultralene foil. The measurements were carried out in three runs at 2-mm steps with down-core and cross-core slits of 2 and 5 mm, respectively, using the following settings: a) 10 kV, 1000 μA, 30 s counting time, no filter; b) 30 kV, 2000 μA, 30 s counting time, Pd-filter; c) 50 kV, 2000 μA, 30 s counting time, Cu-filter. Data processing was carried out with WinAxil version 4.5.6. Element intensities of Al, Br, Si, S, K, Ca, Ti, Cr, Mn, Fe, Zn, Rb, Si, Y, Zr, Nb, Mo, Cd, Sn, Te and Ba were included in the processing. Selected elements are presented as log-ratios of two elements (ln(Ca/Ti), ln(Si/Ti) and ln(Ca/Fe)), in order to minimize closed-sum and matrix effects (Weltje and Tjallingii, 2008; Dunlea et al., 2020). The ln(Si/Ti) ratio is used as proxy for biogenic silica production (Martin-Puertas et al., 2017), and a decrease in ln(Ca/Ti) is applied as an indicator for a change from marine to lacustrine conditions (Røthe et al., 2018). The ln(Ca/Fe) ratio is used as an indicator of changes in minerogenic input and a decrease in the ratio has been suggested to indicate transition from marine to lacustrine conditions (Kylander et al., 2011; Larsen et al., 2017).

After scanning, the lithology of the cores was described. The lithofacies were established according to Eyles et al. (1983), Krüger and Kjær (1999) and Schnurrenberger et al. (2003) and colours were determined based on the Munsell Soil Colour Chart (X-Rite, 2015). The organic matter content was determined based on the loss on ignition (LOI) as described by Heiri et al. (2001). Sediment samples of 1 cm^3 were collected every 2 cm. The samples were dried at 110 °C for 24 h and the organic matter combusted in a muffle furnace at 550 °C for 4 h. The LOI record reveals transitions between organic and minerogenic input. Presence of minerogenic sediments can be used to indicate glacier activity in the catchment area (Karlén and Matthews, 1992; Larsen et al., 2017, 2019; Schomacker et al., 2019).

3.4. Chronology

Eight lacustrine and one marine plant macrofossil samples, as well as three bulk sediment samples were radiocarbon dated at the Ångström Laboratory at Uppsala University, Sweden. Samples from the lowermost section of FMP1 and the middle section of FMP3 were searched for foraminifera, however none were found. All radiocarbon ages were calibrated using CLAM (v. 2.3.5; Blaauw et al., 2020). Age-depth models for cores FMP1 and FMP3 were constructed with the Bayesian-based code BACON (v. 2.3.5; Blaauw, 2010; Blaauw and Christen, 2011) working within the open-source statistical environment R (v. 4.0.2; R Core Team 2020). The IntCal20 and Marine20 calibration curves were used (Heaton et al., 2020; Reimer et al., 2020). The Marine20 curve has a built-in reservoir age, and we apply a local ΔR value of 70 ± 30 years (Mangerud et al., 2006; Mangerud and Svendsen, 2017; Heaton et al., 2020). The reported ages are given in calibrated kiloyears before present (cal. ka BP; BP = 1950), according to Reimer et al. (2020). The core top of FMP1 is assumed to represent the year of sampling, i.e. 2018.

Deglacial and Holocene chronologies from the Woodfjorden and Wijdefjorden region were extracted from the databases SVALHOLA (Farnsworth et al., 2020) and DATED-1 (Hughes et al., 2016). Additionally, we include deglaciation ages not within the databases (Salvigsen and Österholm, 1982; Furrer et al., 1991; Mäusbacher et al., 2002; Gjermundsen et al., 2013; Hormes et al., 2013; Bartels et al., 2017; Braun, 2019; Kjellman et al., 2020). The radiocarbon ages from the databases and the additional ages have been re-calibrated in CLAM with the IntCal20 and Marine20 calibration curves, following the SVALHOLA-standard (local ΔR = 70 ± 30 years).

4. Results

4.1. Lake-floor geomorphology and seismostratigraphy

The large-scale morphology of the lake floor is characterised by multiple ridges and basins (Figs. 4 and 5). Based on acoustic attributes and appearance, three acoustic facies (AF1−3; Figs. 4 and 5) have been identified. The facies were established at well-defined sections and traced laterally in the dataset. Occasional local variations in acoustic appearance and attributes occur. All three facies are identified in both the main basin and the northern sub-basin.

AF1 is the lowermost facies detected in the sub-bottom profiles. It has an undulating upper boundary characterised by a semi-continuous reflection of varying strength. The dominating acoustic appearance is non-transparent, with local semi-transparent parts (Fig. 4). The facies occurs in all acoustic profiles, and the upper boundary is interpreted as the top of bedrock or top of subglacial diamict comparable to similar acoustic facies in fjords and other lakes in Svalbard (Svendsen et al., 1989; Mäusbacher et al.,
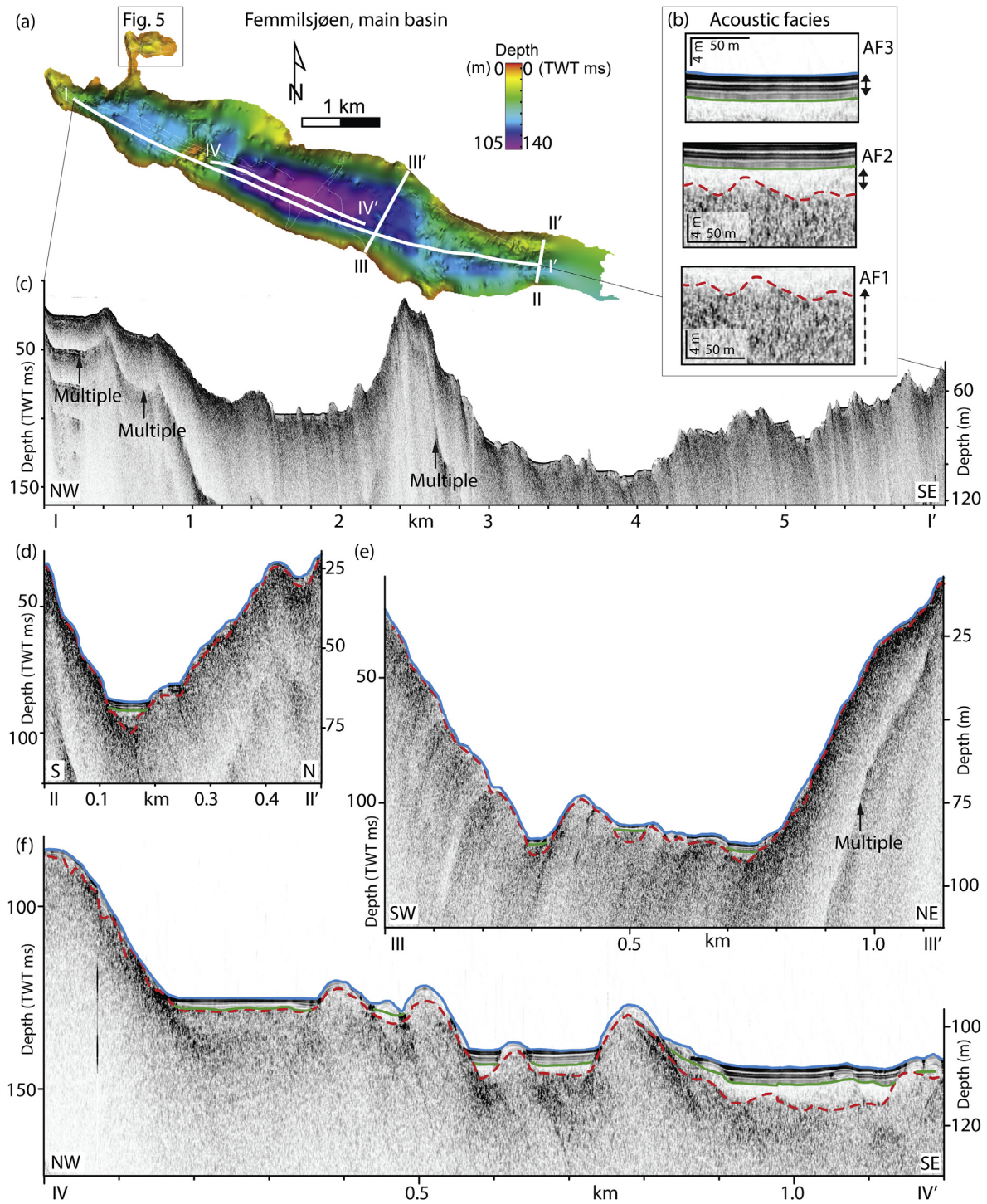
Fig. 4. Geophysical data from Femmilsjøen. (a) Bathymetry showing the main basin and the small northern sub-basin, separated by a sill. Locations of presented sub-bottom-profiles are marked (white lines, c-f), depth in two-way travel time (TWT) and metres (m). (b) Representative sections of the three acoustic facies, AF1 (bedrock/subglacial till), AF2 (glaciomarine sediments) and AF3 (stratified glaciolacustrine sediments), scale in metres. Red, dashed line marks the transition from AF1 to AF2, green line marks the transition from AF2 to AF3, and the blue line marks the seafloor (top of AF3). (c) Profile (I-I') along the main basin of Femmilsjøen, showing the lake floor topography of the two sub-basins and the sill dividing them. (d-e) Cross profiles of the eastern (III-III') and central parts (II-II') of the lake, respectively, with the bounding reflections of the identified acoustic facies. (f) Detailed long profile of the central part of the main basin with the thickest sediment package (IV-IV'). (For interpretation of the references to colour in this figure legend, the reader is referred to the Web version of this article.)

2002; Forwick and Vorren, 2010, Figs. 4 and 5). AF1 reflects the acoustic basement.

AF2 occurs as infill in the depressions of AF1. The facies is semi-transparent, with a diffuse lower but strong upper bounding

reflection. AF2 tapers off towards the slopes of the lake. The facies is up to ~8 m thick (in the deepest part of the main Femmilsjøen basin; Fig. 4). The transparent character indicate massive composition, and it is interpreted as glaciomarine deposits, comparable to
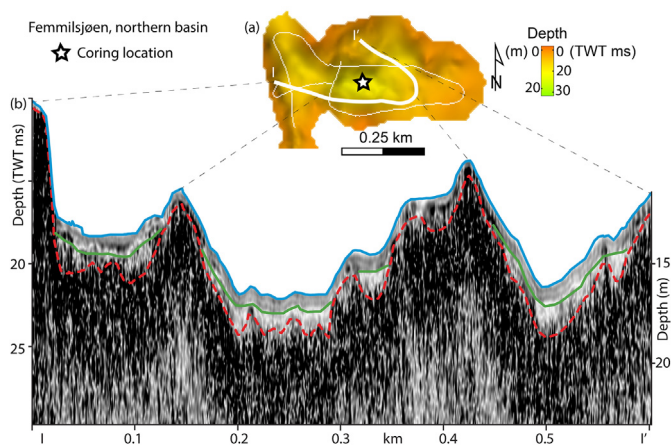
Fig. 5. (a) Detailed bathymetry of the northern sub-basin with the collected sub-bottom profiles (white lines). Thick white line shows the location of the sub-bottom profile shown in (b). Star marks the coring location. (b) Sub-bottom profile with interpretation of seismostratigraphic units (for explanations and colour legend, see Fig. 4). (For interpretation of the references to colour in this figure legend, the reader is referred to the Web version of this article.)

similar acoustic facies in fjords and other lakes in Spitsbergen (Elverhøi et al., 1983; Svendsen et al., 1989; Mäusbacher et al., 2002; Forwick and Vorren, 2010).

AF3 has two to four acoustically stratified, subparallel reflections. The facies also occurs as a ponded infill in the depressions of AF1 and superimposes AF2. Similarly, it tapers towards the lake slopes. The facies is up to ~5 m thick (in the deepest part of the Femmilsjøen basin; Fig. 4). The acoustic stratification reflects changes in lithological composition, comparable to acoustic facies interpreted as glaciolacustrine sediments in other Spitsbergen lakes, and we interpret AF2 as deposited in a glaciolacustrine environment (Svendsen et al., 1989; Mäusbacher et al., 2002).

4.2. Sediment cores − chronology and lithostratigraphy

Six lithofacies (LF1−6) are defined based on lithology, colour as well as physical and chemical properties (Fig. 6). Correlation between the cores is based on lithology, LOI, tie-points in the XRF element log-ratios and X-radiographs (Fig. 7). Correlation (Fig. 7) showed that the upper parts of FMP2 and FMP3 were most likely compressed during coring.

LF1 (108−79.5 cm in core FMP3; Fig. 6) consists of dark grey massive, matrix-supported diamict with abundant outsized clasts (ø ≤ 6 cm). LOI ranges between 1 and 2% and the element log-ratios show large excursions: ln(Ca/Ti) ranges between -3–1.5, ln(Si/Ti) ranges between −0.7–1.6 and ln(Ca/Fe) between -2−0.8. A gradual transition towards weak stratification in the top is visible on the X-radiographs. Datable material was absent, and the organic content was too low for bulk dating. Based on its massive composition, large abundance of clasts, low LOI values and the excursive pattern in the element log-ratios, the facies is interpreted as deposited in a subglacial environment (Svendsen et al., 1989; Larsen et al., 2017). The weak stratification in the top of LF1 indicates a transition from subglacial to marine conditions (Polyak and Solheim, 1994).

LF2 (79.5−25 cm in core FMP3; Fig. 6) consists of dark grey laminated silty clay with occasional clasts (ø ≤ 0.8 cm). The basal contact is gradational, and LOI is generally between 1 and 3%. The element log-ratios are predominantly stable between 79.5 and 42 cm. Negative excursions in all log-ratios occur at ~72 cm, ~33 cm, and ~27 cm. The ~27 cm excursions are associated with a peak LOI value of ~8% at ~27 cm. Marine macroalgae (*Phaeophyceae* indet.)

are abundant between 29 and 19 cm. The X-radiograph shows gradually lower densities towards the top of LF2. Radiocarbon ages from 44.5 cm (bulk) and 28.5 cm (marine macroalgae) yield 16.1 ± 0.3 and 11.4 ± 0.2 cal ka BP, respectively (Figs. 6 and 8; Table 1). Based on its laminated structure, occurrence of clasts, low LOI values and the occurrence of marine macrofossils, this facies is interpreted as deposited in a glaciomarine, glacier proximal environment (e.g., Svendsen et al., 1989; Larsen et al., 2017, 2019). Age-depth modelling (Fig. 8b) indicates that LF2 was deposited prior to 11.5 ± 0.5 cal ka BP.

LF3 (25−13.5 cm in FMP3 and 98.5−76.5 in FMP1; Fig. 6) consists of grey, laminated silty clay. The basal contact is gradational and LOI values vary between 4 and 9%. At the base of the facies in FMP3, large negative excursions occur in all element log-ratios. There is an overall slight decrease in element log-ratios throughout the facies in FMP3, however, the decrease is less pronounced in FMP1. Aquatic bryophytes are abundant and head capsules from adult chironomids have been identified at 21.5 cm and 92.5 cm in FMP3 and FMP1, respectively. A radiocarbon date on aquatic bryophytes from 21.5 cm in FMP3 yields an age of 11.4 ± 0.2 cal ka. BP, whereas a bulk date from FMP1 (92.5 cm) gives an age of 12.1 ± 0.3 cal ka BP (Figs. 6 and 8; Table 1). The laminated structure, marked colour change, slight increase in LOI (compared to LF2), occurrence of aquatic bryophytes and chironomid head capsules, as well as the changes in element log-ratios at the base of the interval together suggest that the transition from LF2 to LF3 represents the isolation of Femmilsjøen from the fjord. We use the decreases in ln(Ca/Fe) and ln(Ca/Ti) as particular indicators of a transition from marine to lacustrine conditions (e.g., Larsen et al., 2017; Røthe et al., 2018). From the LOI values (4−9%) we infer that the minerogenic input is still high, but has decreased compared to LF2. The depositional environment is interpreted as glaciolacustrine (Larsen et al., 2017, 2019; Schomacker et al., 2019). Age-depth modelling indicates that deposition of LF3 commenced just prior to 12.0 ± 0.3 and lasted until *c.* 10.1 ± 0.4 cal ka BP (Figs. 6 and 8; Table 1).

LF4 (13.5−3.5 cm in FMP3 and 76.5−18 cm in FMP1; Fig. 6) consists of dark brown, finely laminated clayey gyttja. The basal contact is sharp and visible in the X-radiographs as a change from higher (dark) to lower (light) densities (Fig. 6). LOI ranges between 4 and 19%. The element log-ratios increase slightly at the base of the facies and again in the central part. A few outsized clasts (ø ≤ 0.5 cm) occur in the lower part of the facies. Aquatic bryophytes and head capsules from both adult and chironomid larvae are abundant throughout the facies. Seven radiocarbon ages (from both cores) on the abundant aquatic bryophytes and one bulk date from FMP1 reveal ages from 10.4 ± 0.2 to 3.4 ± 0.1 cal ka BP (Figs. 6 and 8; Table 1). Based on the laminated structure, high LOI values, and abundance of aquatic bryophytes, this facies is interpreted as deposited in a lacustrine environment (Larsen et al., 2017, 2019; Schomacker et al., 2019). The high LOI indicates increased organic productivity and we interpret the low minerogenic input to reflect limited glacial runoff, and hence limited to no glacial activity in the Femmilsjøen catchment area. The outsized clasts in the lower part of the facies can be explained by seasonal lake ice still forming and rafting material from the lake shores in the early part of the depositional phase of LF4. The clasts disappear after *c.* 9.3 ± 0.4 cal ka BP, ~68 cm in FMP1. Age-depth modelling indicates that LF4 was deposited from 10.1 ± 0.4 to 3.2 ± 0.2 cal ka BP (Figs. 6 and 8; Table 1).

LF5 (exclusively between 18 and 13 cm in FMP1; Fig. 6) consists of light grey laminated silty clay. The basal contact is sharp and seen as changes from lower to higher densities on the X-radiographs, as well as a colour change from dark brown to light grey. The laminae are slightly thicker than in LF4. LOI decreases from 12% at the lower boundary to 4% in the top of the unit. The ln(Ca/Ti) and ln(Ca/Fe)
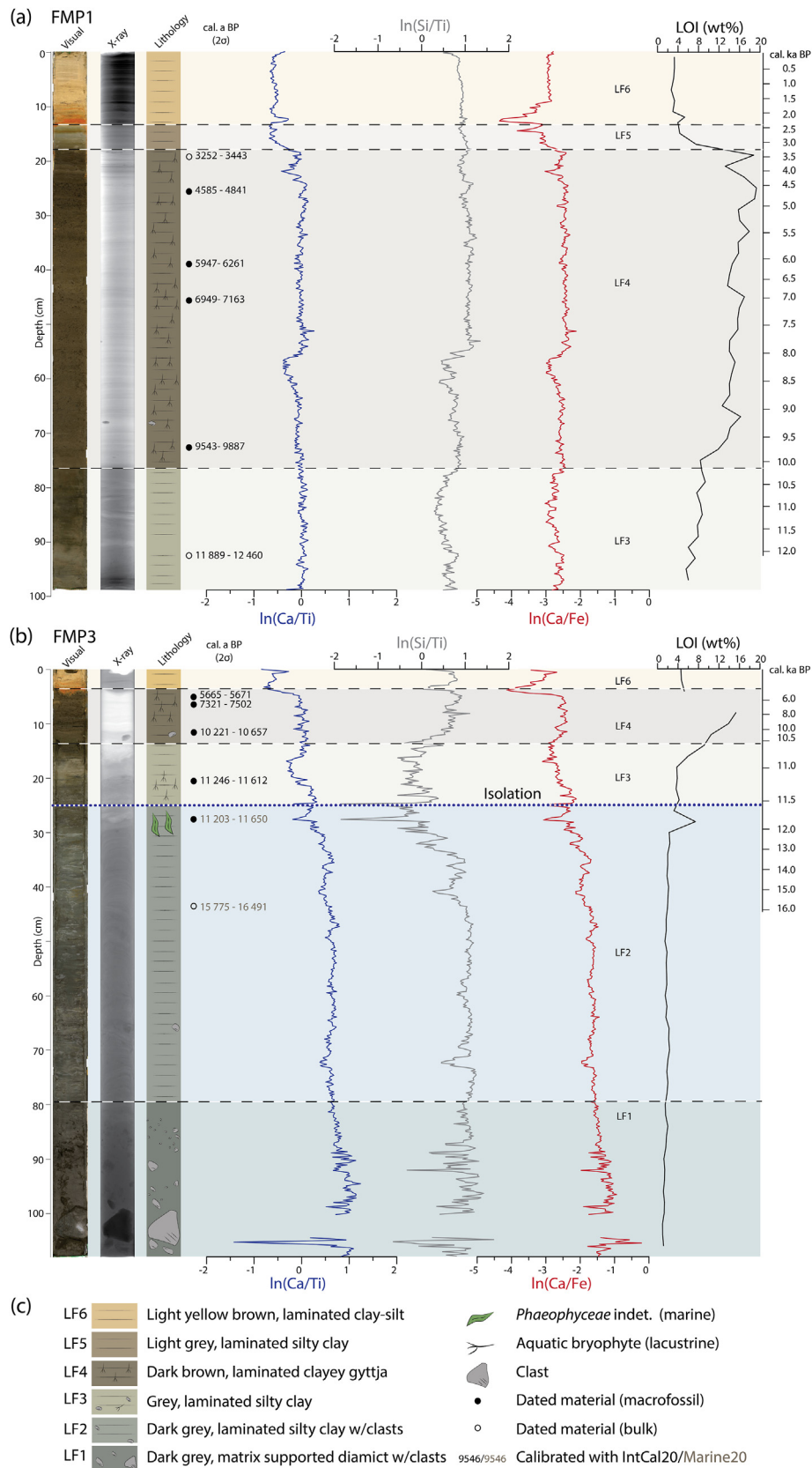
Fig. 6. Composite logs of cores FMP1 (a) and FMP3 (b): core photograph, X-ray image, lithological log, calibrated 2σ age range (in cal. a BP), physical and element properties, as well as LOI. Lithostratigraphic units are indicated. Median ages from BACON (cal. ka BP) to the right. Suggested time of isolation is marked on (b) with white/blue dotted line. (c) Legend. (For interpretation of the references to colour in this figure legend, the reader is referred to the Web version of this article.)
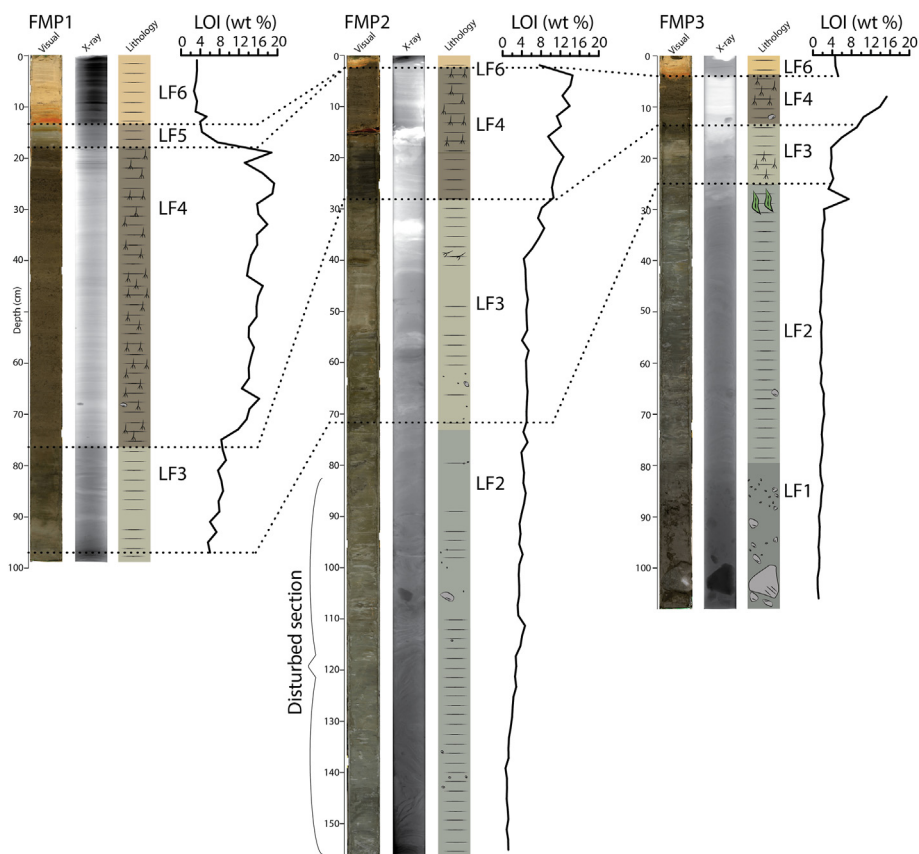
Fig. 7. Correlation of the three sediment cores FMP1, FMP2 and FMP3. Core photograph, X-ray image, lithological log and LOI. For legend see Fig. 6c.

ratios decrease, whereas the ln(Si/Ti) ratio remains stable throughout the facies. Datable material was absent in this facies. Based on the colour change, decreasing LOI and element log-ratios, LF5 is interpreted as deposited in a lacustrine environment with increasing minerogenic input due to glacier growth in the Femmilsjøen catchment area (Larsen et al., 2017, 2019; Schomacker et al., 2019). Age-depth modelling suggests that deposition of L5 took place from 3.2 ± 0.2 to 2.1 ± 0.7 cal ka BP (Figs. 6 and 8; Table 1).

LF6 (13−0 cm in FMP1 and 3.5−0 cm in FMP3; Fig. 6) consists of light yellow brown laminated clay-silt. The basal contact is sharp and seen in the X-radiograph as a change to higher densities (darker) than in LF5. An orange layer concurrent with positive ln(Ca/Ti) and negative ln(Ca/Fe) excursions marks the base of the facies. The LOI is ~4% throughout LF6 and datable material was absent in this facies. However, the sediment-water interface was preserved in FMP1 during coring, and therefore, we assume that the top sediments in LF6 in FMP1 are of modern age. Based on the lithology, colour and low LOI, this facies is interpreted as deposited in a glaciolacustrine environment with high minerogenic input (e.g., Larsen et al., 2017; 2019; Schomacker et al., 2019). We interpret the enhanced minerogenic input as indicative of further glacier growth in the catchment. Age-depth modelling indicates that deposition of LF6 took place from 2.1 ± 0.7 cal ka BP until present (Figs. 6 and 8; Table 1).

4.3. Correlation between acoustic facies and lithofacies

AF1 is interpreted as top of bedrock or top of subglacial diamict (Figs. 4 and 5). Based on the occurrence of the diamict (LF1) in the lowermost part of FMP3 (Fig. 6) it is likely that the uppermost part

of AF1 partly constitutes subglacial diamict (Svendsen et al., 1989; Mäusbacher et al., 2002). We interpret AF2 to correlate with LF2 (laminated glaciomarine deposits). Despite being correlated to the laminated lithostratigraphic unit, AF2 appears predominantly transparent, explained by the fact that laminae thicknesses are below the vertical resolution of the acoustic signal of the sub-bottom profiler (Svendsen et al., 1989; Mäusbacher et al., 2002). AF3 correlates with LF3−6 (glaciolacustrine, lacustrine and glacio-lacustrine facies; comparable to facies in other Spitsbergen lakes; Svendsen et al., 1989; Mäusbacher et al., 2002). In the bathymetric lows (Figs. 4 and 5), AF3 has up to four subparallel reflections and we interpret each sub-reflection to correspond to one lithofacies each.

5. Discussion

5.1. Late Weichselian − from full glacial conditions to deglaciation

From the presence of LF1 (subglacial diamict; and potentially the upper part of AF1) we infer that the Femmilsjøen area was covered by grounded ice during the Late Weichselian (Fig. 9a), in agreement with observations from the northern part of Wijdef-jorden (Allaart et al., 2020). The lowermost bulk age from Femmilsjøen indicates deglaciation prior to 16.1 ± 0.3 cal ka BP (Figs. 6 and 8; Table 1), and based on our interpretation of the time of isolation, this facies (LF2) is of marine origin. Bulk ages of marine sediments should be treated cautiously, as reworked carbon can cause apparently older ages (Licht et al., 1998; Howe et al., 2008; Hogan et al., 2010). Considering the low LOI (~2%) at the depth of the bulk date, even small amounts of inert carbon in the bulk
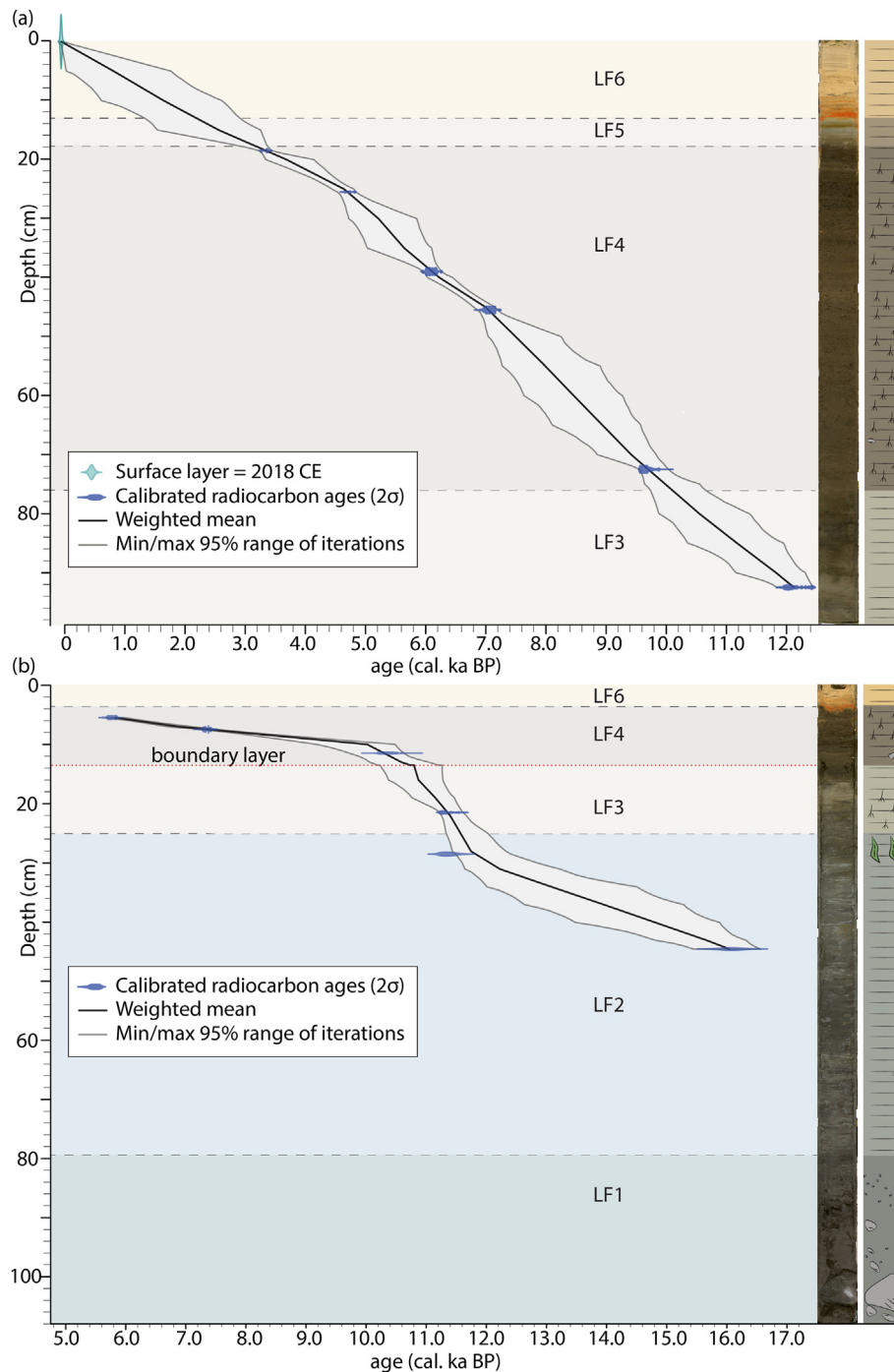
Fig. 8. Age-depth models of cores FMP1 (a) and FMP3 (b). Core photographs and lithological logs to the right. The age of the FMP1 core top is set to 2018 CE (year of coring). See Fig. 6 and Table 1 for details about the radiocarbon ages.

sample, could introduce significant errors in the radiocarbon age (Walker, 2005). However, the amount of limestone in the Femmilsjøen catchment is very limited, and the age largely agrees with the regional deglaciation ages (Fig. 10).

The continental shelf north of Wijdefjorden is narrow, and the (last) deglaciation is likely to have happened fast (Hogan et al., 2017). The mouths of Woodfjorden and Wijdefjorden deglaciated prior to 15.2 ± 0.3 and 12.0 ± 0.3 cal ka BP, respectively (Bartels et al., 2017; Allaart et al., 2020; Farnsworth et al., 2020, Fig. 10). The extrapolation by Allaart et al. (2020) suggests that the mouth of

Wijdefjorden deglaciated at least prior to 14.5 ± 0.3 cal ka BP. Exposure ages reveal glacier free mountain plateaus (400 m a.s.l.) on the eastern side of Wijdefjorden already between 17.7 ± 1.2 and 18.3 ± 1.2 ka ago, indicating that thinning commenced prior to this (Hormes et al., 2013, Fig. 10). Lake sedimentary records from Vårfluesjøen and Vogtvatnet, located on the peninsula west of Wijdefjorden, suggest deglaciation prior to 13.1 ± 0.3 and 13.7 ± 0.3 cal ka BP, respectively (Mäusbacher et al., 2002; Røthe et al., 2018, Fig. 10) and an age from raised marine sediments in inner Liefdefjorden (tributary to Woodfjorden, Fig. 10) indicate deglaciation

Table 1
Radiocarbon ages from Femmilsjøen, Svalbard. Laboratory IDs for samples of marine origin are written in bold. The IntCal20 and Marine20 calibration curves (Heaton et al., 2020; Reimer et al., 2020) are used for calibration. The Marine20 curve has a built-in reservoir age, and we apply a local ΔR value of 70 ± 30 years (Mangerud et al., 2006; Mangerud and Svendsen, 2017). The measured ^{14}C age, the calibrated 2σ age range, the calibrated median age, as well as the BACON modelled median age are given.

Lab ID	Core	Lithofacies	Depth(cm)	Dated material	δ^{13} C ‰ VPDB	^{14}C age(a BP)	Calibrated 2σ age range(cal. a BP)	Calibrated median age (cal. a. BP)	BACON modelled median age (cal. a BP)
Ua-66429	FMP1	LF4	18.5	bulk	−34.8	3132 ± 27	3252−3297 3325−3404 3427−3443	3360	3359
Ua-64439	FMP1	LF4	25.5	aquatic bryophyte	−26.6	4192 ± 35	4585−4597 4616−4766 4785−4841	4727	4707
Ua-64440	FMP1	LF4	39	aquatic bryophyte, whole	−26.9	5309 ± 39	5947−5962 5992−6199 6252−6261	6087	6115
Ua-64441	FMP1	LF4	45.5	aquatic bryophyte	−28.5	6164 ± 40	6949−7163	7063	7044
Ua-64442	FMP1	LF4	72.5	aquatic bryophyte	−29.2	8705 ± 43	9543−9781 9848−9887	9649	9672
Ua-64443	FMP1	LF3	92.5	bulk	−24.3	10,311 ± 39	11,889−11,895 11,934−12,196 12,226−12,270 12,299−12,329 12,349−12,460	12,089	12,088
Ua-66430	FMP3	LF4	5.5	aquatic bryophyte	−26.4	5069 ± 43	5665−5671 5716−5916	5815	5829
Ua-64449	FMP3	LF4	7.5	aquatic bryophyte	−26.3	6505 ± 42	7321−7502	7390	7382
Ua-66431	FMP3	LF4	11.5	aquatic bryophyte	−	9225 ± 101	10,221−10,604 10,616−10,657	10,406	10,332
Ua-64450	FMP3	LF3	21.5	aquatic bryophyte	−27.4	9953 ± 42	11,246−11,412 11,419−11,505 11,526−11,612	11,371	11,336
Ua-64451	FMP3	LF2	28.5	*Phaeophyceae* indet.	−27.4	10,469 ± 42	11,203−11,650	11,409	11,767
Ua-64438	FMP3	LF2	44.5	bulk	−24.5	14,108 ± 108	15,775−16,491	16,123	16,073

prior to 13.0.±0.2 cal ka BP (Furrer et al., 1991). As such, we infer that Femmilsjøen was deglaciated early, potentially prior to 16.1 ± 0.3 cal ka BP, which implies that it deglaciated prior to Vogtvatnet, Vårfluesjøen and Linnévatnet (Svendsen and Mangerud, 1997; Mäusbacher et al., 2002; Røthe et al., 2018, Figs. 1 and 10). LF2 and AF2 were deposited during the deglaciation phase in a marine glacier-proximal setting (Fig. 9b), where seawater temperatures and the amount of sea ice fluctuated repeatedly (Allaart et al., 2020).

5.2. Early Holocene - isolation from the marine environment

Femmilsjøen was inundated by the sea after deglaciation and subsequently became isolated due to glacioisostatic rebound; LF3 and the lowermost part of AF3 were deposited during the isolation phase (Figs. 9c, 10 and 11). In core FMP3, close to the upper boundary of LF2, we identified a layer with marine macroalgae (*Phaeophyceae* indet; 28.5 cm) that dated to 11.4 ± 0.2 cal ka BP. In LF3 aquatic bryophytes at 21.5 cm dated to 11.4 ± 0.2 cal ka BP, and head capsules from adult chironomids, indicative of lacustrine conditions, occur (Fig. 6; Table 1). In FMP1, the lowermost bulk age from LF3 provides an age of 12.1 ± 0.3 cal ka BP. The macrofossils suggest that the interval between 27.5 and 20.5 cm in FMP3 (11.7 ± 0.3 to 11.3 ± 0.2 cal ka BP) reflects the isolation (Fig. 6; Table 1). However, the outlet and marine isolation threshold of Femmilsjøen constitutes a ~50 m wide channel, incised ~12 m into the surrounding bedrock (Fig. 3b). Compared to fluvial incision rates of 0.15 m ka^{-1} in similarly resistant bedrock (Schildgen et al., 2002), it is unlikely that the outlet channel has been incised only during the course of the Holocene. Therefore, we assume that the majority of the incision is of pre-Holocene age, and the lake isolation threshold, constituted by the bottom of the outlet channel, a valid sea-level index point. The ridge surrounding the 50-m-wide channel most likely restricted the water exchange between

Wijdefjorden and Femmilsjøen a while prior to the final isolation. The decreasing ln(Ca/Ti) ratio in FMP3 from ~35 cm (*c.* 13.4 ± 1.1 cal ka BP) towards the top of LF2 and throughout LF3 (Fig. 6) indicates a gradual transition from marine to lacustrine conditions, similar to observations in Vårfluesjøen (Røthe et al., 2018). We interpret the presence of marine macroalgae as indicators for saline water dominating the Femmilsjøen basin until the top of LF2.

We suggest that the isolation phase of Femmilsjøen occurred gradually and that a period with brackish water conditions in the basin prevailed from *c.*13.4 cal ka BP (Fig. 11). The final isolation most likely occurred between 11.7 ± 0.3 (27.5 cm in FMP3) and 11.3 ± 0.2 cal ka BP (20.5 cm in FMP3). Isolation between 11.7 ± 0.3 to 11.3 ± 0.2 cal ka BP is comparable to the regional postglacial uplift rate and agrees with the relative sea level curve from Salvigsen and Österholm (1982; Fig. 11). After the isolation, minerogenic sedimentation dominated until 10.1 ± 0.4 cal ka BP (during deposition of LF3). Thus, we infer that glaciers existed in the Femmilsjøen catchment area at this time, with a more distal glacier compared to during deposition of LF2.

On the peninsula west of Wijdefjorden, radiocarbon ages of reworked mollusc shells in moraines range from 11.6 ± 0.3 to 10.9 ± 0.3 (Fig. 10; Farnsworth et al., 2020). The moraines are interpreted as formed by re-advances of tributary glaciers during the Early Holocene, after retreat of the main glacier occupying Woodfjorden. The moraines are comparable to Early Holocene glacier advances seen elsewhere in Svalbard (Lønne 2005; Larsen et al., 2018; Farnsworth et al., 2017, 2018, Fig. 10) and the ages are comparable with the age of LF2 indicating that glaciers were still active during the overall deglaciation.

5.3. Early to Middle Holocene - the Holocene Thermal Maximum

LF4 contains relatively little minerogenic material, which can be interpreted in two ways, both indicating that the Åsgardfonna Ice
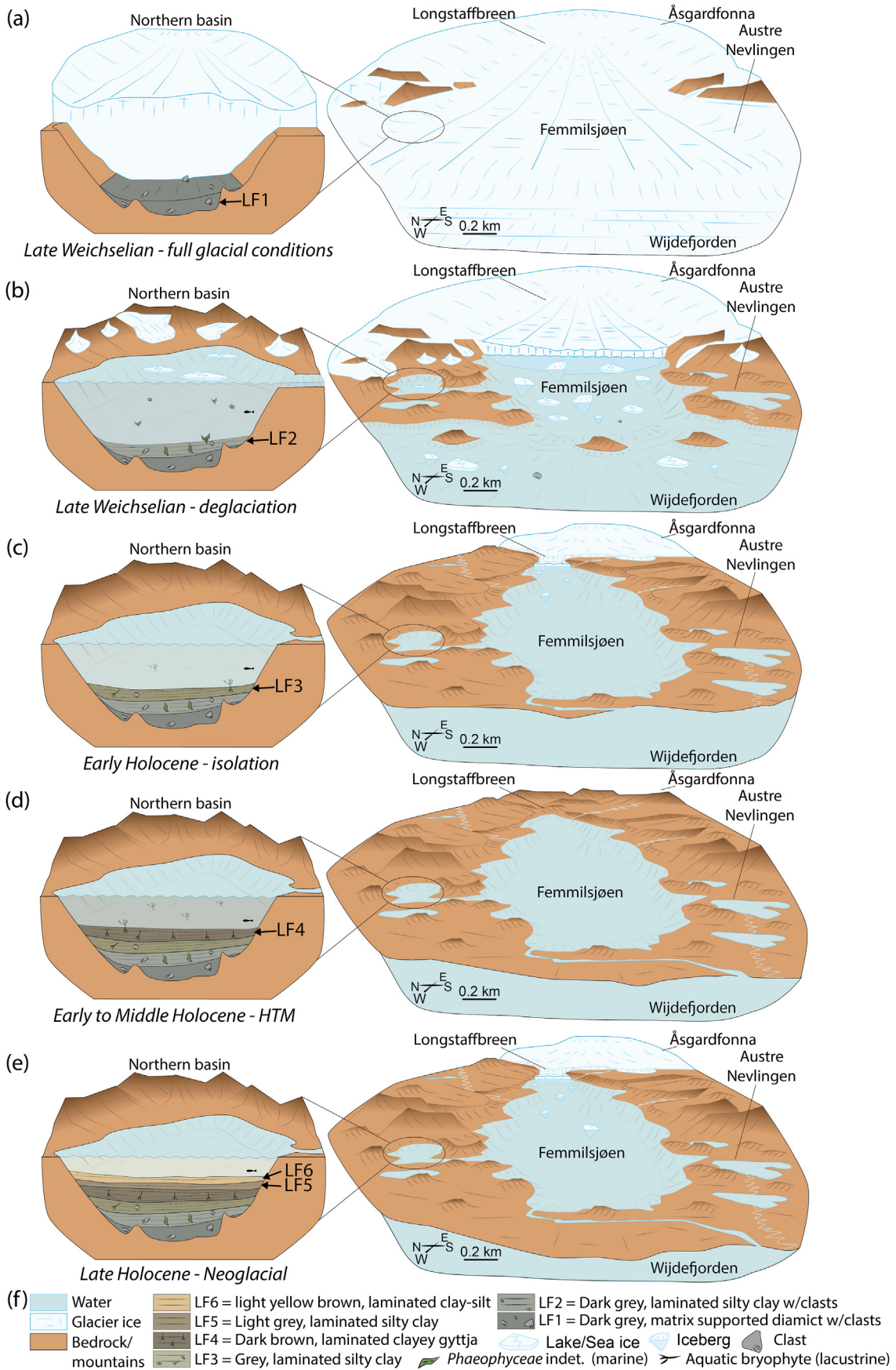
Fig. 9. Conceptual model of the depositional environment in Femmilsjøen from Last Glacial Maximum until present. (a) Late Weichselian − full glacial conditions. (b) Late Weichselian − deglaciation, marine conditions. (c) Early Holocene − isolation of Femmilsjøen. (d) Early to Middle Holocene - Holocene Thermal Maximum. (e) Late Holocene - Neoglacial. (f) Legend.
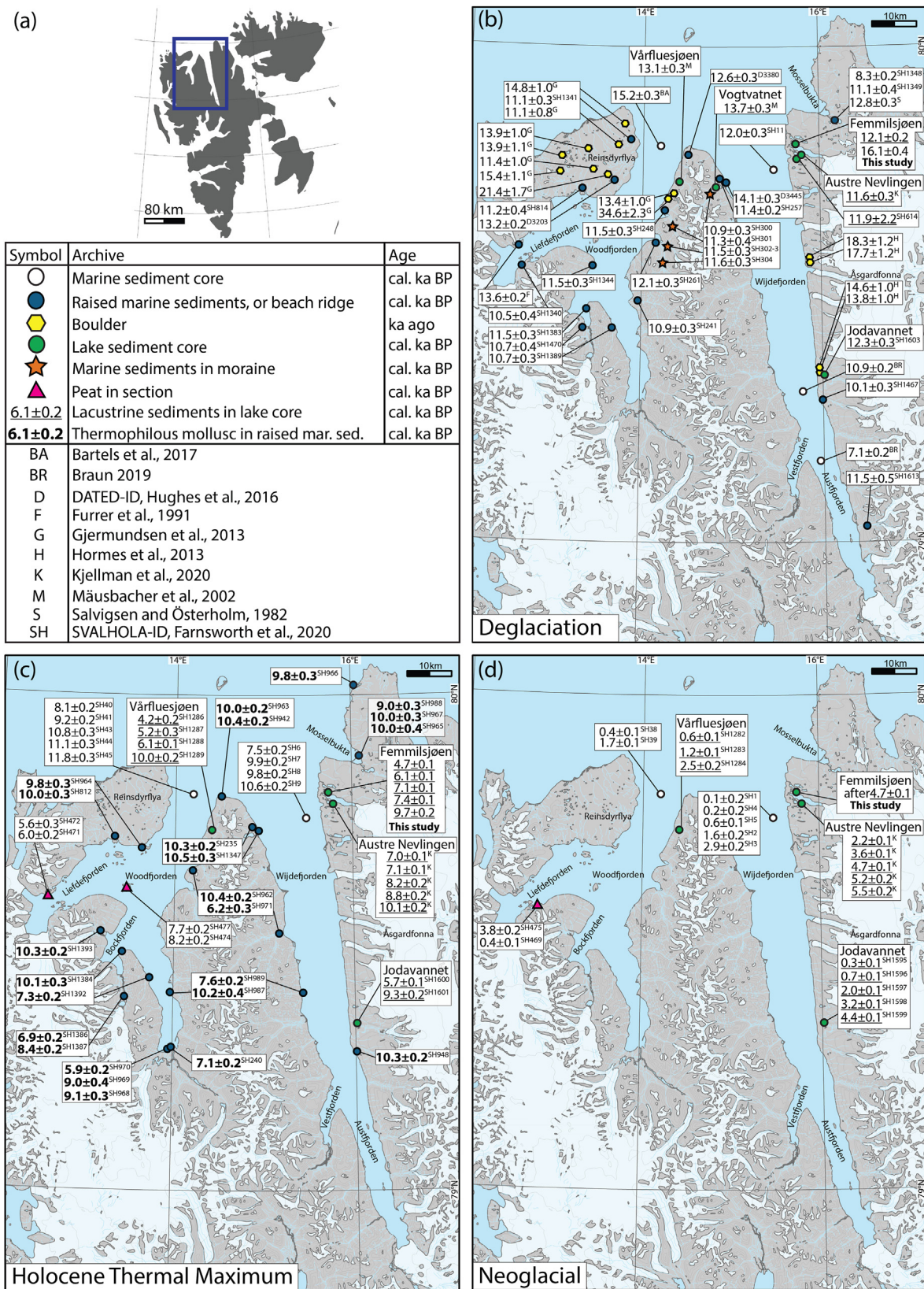
(a)

80 km

Symbol	Archive	Age
○	Marine sediment core	cal. ka BP
● (blue)	Raised marine sediments, or beach ridge	cal. ka BP
⬡ (yellow)	Boulder	ka ago
● (green)	Lake sediment core	cal. ka BP
★ (orange)	Marine sediments in moraine	cal. ka BP
▲ (pink)	Peat in section	cal. ka BP
6.1±0.2 (underlined)	Lacustrine sediments in lake core	cal. ka BP
6.1±0.2 (bold)	Thermophilous mollusc in raised mar. sed.	cal. ka BP
BA	Bartels et al., 2017	
BR	Braun 2019	
D	DATED-ID, Hughes et al., 2016	
F	Furrer et al., 1991	
G	Gjermundsen et al., 2013	
H	Hormes et al., 2013	
K	Kjellman et al., 2020	
M	Mäusbacher et al., 2002	
S	Salvigsen and Österholm, 1982	
SH	SVALHOLA-ID, Farnsworth et al., 2020	

(b) Deglaciation

(c) Holocene Thermal Maximum

(d) Neoglacial

Fig. 10. (a) Inset map with blue square indicating the location of (b-d). (b-d) Maps with all previously published deglacial to Holocene chronologies from the Wijdefjorden and Woodfjorden areas (marine, terrestrial and lacustrine archives). The DATED-1 and SVALHOLA databases (Hughes et al., 2016; Farnsworth et al., 2020) form the basis for the map; separate references for chronologies not included in the databases, are marked/noted. (For interpretation of the references to colour in this figure legend, the reader is referred to the Web version of this article.)
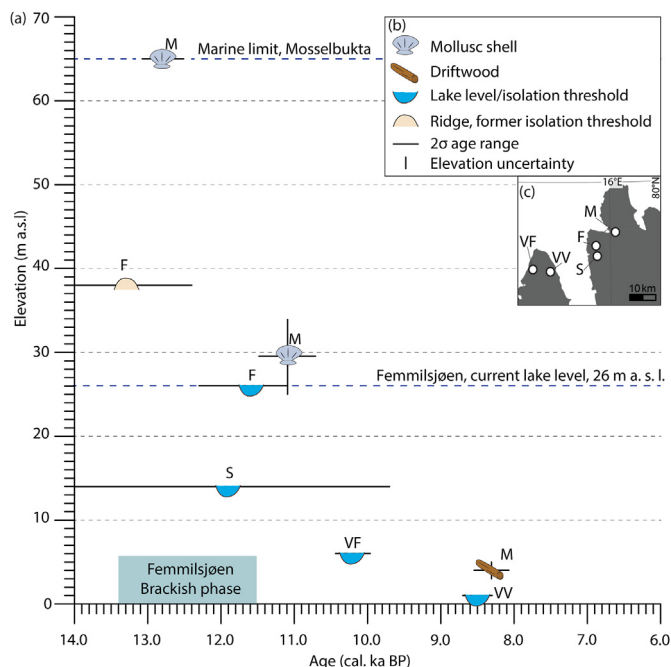
Fig. 11. (a) Regional postglacial uplift indicated by isolation basins (blue lake symbols) and occurrence of driftwood and mollusc shells in raised beach ridges, modified after Salvigsen and Österholm (1982). Current surface level of Femmilsjøen is marked with a dashed, blue line. M = Mosselbukta (Fig. 10; SH1348-SH1349; Farnsworth et al., 2020; Salvigsen and Österholm, 1982), F = Femmilsjøen (this study), S = Strøen (Fig. 10; SH-614, Farnsworth et al., 2020), VF = Vårfluesjøen and VV = Vogtvatnet (Fig. 10; Mäusbacher et al., 2002; Røthe et al., 2018). (b) Legend. (c) Inset map of NE Spitsbergen shows site locations. (For interpretation of the references to colour in this figure legend, the reader is referred to the Web version of this article.)

Cap was significantly smaller than today during deposition of this facies (10.1 ± 0.4 to 3.2 ± 0.2 cal ka BP; Fig. 9d). One interpretation is that the Åsgardfonna Ice Cap was a considerably smaller ice cap, and that limited to no glacial runoff reached Femmilsjøen (Fig. 2). The other interpretation is that the lake level lowered as a result of decreased runoff, and thus caused reduced sediment supply to the northern sub-basin. We assume that the main transport mechanism of sediment from the fluvial and glacial input sources (in the eastern end of the main basin and from there into the northern sub-basin) is by suspension in inter- and overflows and/or ice rafting (Smith and Ashley, 1985). Relative emergence of the present day 5 m deep threshold separating the two basins, could limit the supply of interflow-suspended sediment to the sub-basin or lead to complete isolation of the northern sub-basin from the main basin. However, based on leaf wax hydrogen isotope analyses on lake sediments from Austre Nevlingen (Figs. 1–3); Kjellman et al. (2020) suggested increased winter precipitation during the Early Holocene/HTM. They inferred this increase to be a result of regional warming, reduced sea-ice cover in surrounding waters and greater winter ocean evaporation. Higher winter precipitation amounts would result in greater runoff to Femmilsjøen during spring snowmelt. Hence, we find it highly unlikely that the water level in Femmilsjøen would drop 5 m, to either isolate the northern sub-basin, or restrict the water flow from the main lake basin during the entire period from 10.1 ± 0.4 to 3.2 ± 0.2 cal ka BP. Furthermore, the same acoustic facies (even though of various thickness; Figs. 4 and 5) appear in both the main and the northern sub-basin, indicating similar sediment supply across the entire lake during the course of the deglaciation and Holocene. Therefore, we favour the first interpretation: the organic-rich facies LF4 (deposited from 10.1 ± 0.4 to 3.2 ± 0.2 cal ka BP; Fig. 6) represents a period with very

limited to no glacial runoff in the Femmilsjøen catchment and a greatly reduced to absent Åsgardfonna (Fig. 9d). Furthermore, we suggest that the northern sub-basin was connected to the main Femmilsjøen basin throughout the Holocene.

Voldstad et al. (2020) suggested an early HTM in the Wijdefjorden area, evident by distinctly thermophilous plant species in Jodavannet (Ringhorndalen, central Wijdefjorden; Fig. 1) by 11.2–10.9 cal ka BP. Spring sea-ice minimum and coinciding water temperature maximum between *c.* 10–7 cal ka BP at the mouth of Wijdefjorden point towards warm waters during the HTM (Allaart et al., 2020). This is supported by high subsurface temperatures and reduced sea-ice cover in eastern Fram Strait during the same period (Werner et al., 2016). Thermophilous molluscs (ages ranging from 10.5 ± 0.3 to 5.9 ± 0.2 cal ka BP) occur in Woodfjorden and Wijdefjorden simultaneously with the onset of deposition of LF4 (Mangerud and Svendsen, 2018, Fig. 10). The oldest of these mollusc shells was found in the outer part of Wijdefjorden, close to Vogtvatnet (Mangerud and Svendsen, 2018; Farnsworth et al., 2020, Fig. 10). Peat layers in geological sections in Liefdefjorden (a tributary to Woodfjorden; Fig. 10) yield ages from 5.6 ± 0.3 to 8.2 ± 0.2 cal ka BP and indicate warm conditions. The increase in the ln(Si/Ti) ratio (at ~56 cm in FMP1, corresponding to a median age of 8.1 ± 0.7 cal ka BP) could indicate an increase in biogenic silica production (Martin-Puertas et al., 2017), reflecting beneficial living conditions for silica producing diatoms in Femmilsjøen during the HTM. Relatively low sedimentation rates in Wijdefjorden and the neighbouring fjords during HTM are interpreted as indicative of very little glacial activity during the HTM (Flink et al., 2017; Bartels et al., 2017, 2018; Allaart et al., 2020).

Early Holocene glaciers retreated from the Femmilsjøen catchment, suggesting that the enhanced winter precipitation (Kjellman et al., 2020) was out-balanced by the combination of high summer insolation as well as warm terrestrial and marine conditions. Hence, we infer that the Early Holocene glacier mass balance primarily was controlled by summer ablation (similar to today and comparable to Early Holocene glaciers in southwest Greenland; Larsen et al., 2017; Hanssen-Bauer et al., 2019).

We infer that the HTM and associated glacier minimum of the Åsgardfonna Ice Cap occurred between 10.1 ± 0.4 and 3.2 ± 0.2 cal ka BP. The NW part of the Åsgardfonna Ice Cap was most likely very small or absent (Fig. 9d). The glacier-free conditions recorded in the Femmilsjøen catchment during the HTM is comparable to catchments of smaller glaciers and ice caps spread along the western and northern coasts of Svalbard (Fig. 12; Svendsen et al., 1987; Svendsen and Mangerud 1997; Snyder et al., 2000; Mäusbacher et al., 2002; Røthe et al., 2015, 2018; van der Bilt et al., 2015; de Wet et al., 2018; Schomacker et al., 2019). It is also in agreement with modelling results suggesting that glacier ice in Svalbard only survived the HTM in the north-eastern and eastern parts of Svalbard (Fjeldskaar et al., 2018). However, the glacier minimum commenced 4.0 to 0.5 ka earlier in the Femmilsjøen catchment than elsewhere in Svalbard (Figs. 2 and 12), maybe related to the proximity of northern Wijdefjorden and Femmilsjøen to the shelf break. Atlantic Water was present in Hinlopen Trough already by *c.* 15.0 cal ka BP (Ślubowska et al., 2005). The narrow shelf and lack of a sill at the mouth of Wijdefjorden most likely allowed for early intrusion of Atlantic Water through Hinlopen Trough into Wijdefjorden and evoked rapid glacial retreat (Koç et al., 2002; Ślubowska et al., 2005; Batchelor et al., 2011; Allaart et al., 2020). The presence of warm Atlantic Water in Wijdefjorden, together with peak insolation could provide warm enough boundary conditions to initiate an early regional onset of the HTM in the already deglaciated area around Femmilsjøen.

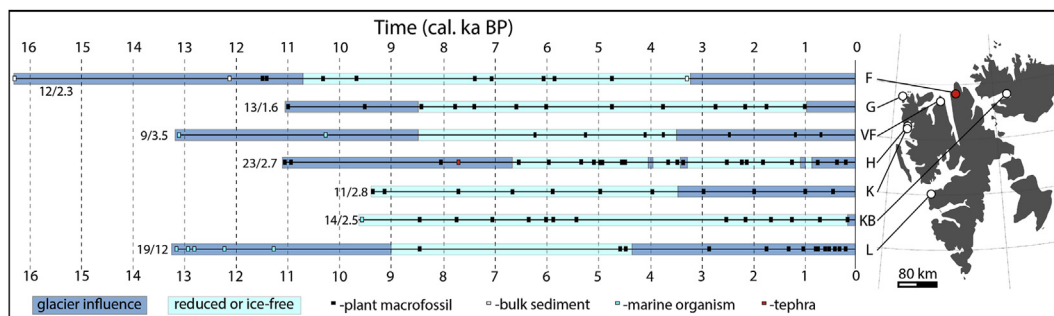It seems that the NW part of Åsgardfonna behaved differently

Fig. 12. Diagram highlighting the age and distribution of dates from glacial lake sediment records on Svalbard showing the times of deglaciation, the periods with absent glacial signals and highlighting the onset of the Neoglaciation. Terrestrial or aquatic plant macrofossils (black boxes), crypto-tephra (red boxes), marine mollusc shells and foraminifera (blue boxes), as well as bulk sediment ages (white boxes) are used to constrain core chronologies. Values to the left of the chronologies indicate the number of dates and the composite core length (in meters) of each sediment core. Inset map shows the location of the core sites: F = Femmilsjøen (this study), G = Gjøavatnet (de Wet et al., 2018), VF = Vårfluesjøen (Mäusbacher et al., 2002; Røthe et al., 2018), H = Hajeren (van der Bilt et al., 2015) only the Late Glacial and Holocene part of this core is included here, K = Kløsa (Røthe et al., 2015), KB = Kløverbladvatna (Schomacker et al., 2019), L = Linnévatnet (Svendsen et al., 1987; Svendsen and Mangerud, 1997; Snyder et al., 2000). (For interpretation of the references to colour in this figure legend, the reader is referred to the Web version of this article.)

than larger tidewater glaciers and ice caps in central Spitsbergen, that survived the HTM, based on the sustained occurrence of IRD throughout the Holocene (Hald et al., 2004; Forwick and Vorren, 2009; Baeten et al., 2010; Rasmussen et al., 2013). However, a new study from Dicksonfjorden (inner Isfjorden; Joo et al., 2019) argue that most of the IRD occurring in Dicksonfjorden is sea-ice and not glacier ice rafted, and could challenge the paradigm that tidewater glaciers in central Spitsbergen survived the HTM.

5.4. Late Holocene - the Neoglacial

In Femmilsjøen, glaciolacustrine sediments reoccur in LF5, presumably representing glacier growth in the catchment area from c. 3.2 ± 0.2 cal ka BP (Fig. 9e). This age is comparable to ages (c. 3.5 cal ka BP) from Vårfluesjøen and Kløsa (Figs. 10 and 12; Mäusbacher et al., 2002; Røthe et al., 2015, 2018). In Jodavannet, a distinct shift in lithology and sedaDNA data at c. 4.4 ± 0.1 cal ka BP is attributed to Neoglacial cooling and enhanced nivation processes within the catchment (Fig. 1; Voldstad et al., 2020). The lag in the onset of the Neoglacial between Femmilsjøen and Jodavannet might be a function of Jodavannet having a more continental climate; however, we believe the lithological changes at both sites reflect Neoglacial cooling. The onset of the glacier re-growth of Åsgardfonna corresponds well with the high sediment accumulation rate observed for the similar time interval in a marine core in northern Wijdefjorden off the outlet from Femmilsjøen (Allaart et al., 2020). Furthermore, the marine record shows increased spring sea-ice extent and decreasing seawater temperatures from c. 3.1 cal ka BP (Allaart et al., 2020) and similar cooling occurs in other fjords in northern Svalbard (Bartels et al., 2017, 2018; Flink et al., 2017). In Liefdefjorden, vegetation kill ages from entombed in-situ peat layers yield ages from 3.8 ± 0.2 to 0.4 ± 0.1 cal ka BP, indicating that Neoglacial glacier expansion commenced after 3.8 ± 0.2 cal ka BP (Fig. 10; Furrer et al., 1991; Farnsworth et al., 2020).

The glacier growth in the Femmilsjøen catchment, the buried and glacially overridden peat in Liefdefjorden, as well as the cooling in the northern part of Wijdefjorden mark the onset of the Neoglacial in northern Spitsbergen. The glaciers in northern Spitsbergen were likely responding to decreasing summer temperatures and less ablation (Laskar et al., 2004). This is comparable to the modern mass-balance observations on Svalbard showing that the glaciers mainly respond to changes in summer temperature (Hagen et al., 2002; Marlin et al., 2017; Hanssen-Bauer et al., 2019) and comparable to Late Holocene glaciers in SW Greenland (Larsen

et al., 2017).

Due to the continuous dominance of minerogenic sediments in LF6, we infer that the Åsgardfonna Ice Cap reached a size as large as, or even larger than the modern glacier configuration around the onset of LF6 (2.1 ± 0.7 cal ka BP). This implies that the glaciers in the Femmilsjøen catchment grew to their full Neoglacial extent within c. 1.1 ka (from 3.2 ± 0.2 to 2.1 ± 0.7 cal ka BP; Fig. 9e).

The sediment-water interface was preserved in FMP1 during coring, and we assume that the top sediments are modern. LF6 thus represents the modern depositional environment. Today, the surge-type glacier Longstaffbreen has a calving margin terminating into the eastern end of the lake. We assume that Longstaffbreen has dominated the sediment supply into the lake during the last c. 2.1 cal ka BP, and that its margin, like today, terminated in the lake or in the near vicinity onshore.

5.5. Åsgardfonna in a Circum-Arctic perspective

Femmilsjøen holds a continuous, deglacial to Holocene lacustrine sedimentary record of the Åsgardfonna Ice Cap, which is rare in the Arctic (Briner et al., 2016). To place our findings in a Circum-Arctic perspective, we compare them to climate records covering the same time interval from smaller glaciers and ice caps from the Canadian Arctic, Greenland, and the Russian Arctic. In the Femmilsjøen area the glacier minimum and HTM seem to occur simultaneously, however, it may differ across the Circum-Arctic region.

The marine-based Svalbard-Barents Sea Ice Sheet disintegrated rapidly, attributed to early (from c. 15.0 cal ka BP) advection of Atlantic Water to Svalbard from the West Spitsbergen Current. This led to debuttressing of ice shelves, as a result of oceanic absorption of the orbitally forced atmospheric warming at the transition to the Holocene (Ślubowska et al., 2005; Hormes et al., 2013; Hogan et al., 2017). By comparison, there was still residual ice from the last Laurentide Ice Sheet on the North American continent until c. 8.0 cal ka BP, and freshwater releases from this ice caused regional cooling and influenced the glaciers and ice caps in the Canadian Arctic (Kaufman et al., 2004; Briner et al., 2016). The same applies to northern and western Greenland, where the ice sheet still today affects the regional climate (Briner et al., 2016).

In the Canadian Arctic and Greenland, maximum warmth and glacier minima generally occurred between c. 9.0 and 5.0 cal ka BP (Briner et al., 2016; Larsen et al., 2019). In the Russian Arctic archipelagos Franz Josef Land and Severnaya Zemlya (Fig. 1), the glaciers were already smaller than present between c. 12.5 and

10.6 cal ka BP, and the climate was warmer than today from *c.* 11.5 to 9.5 cal ka BP (Solomina et al., 2015). The glacial input in Femmilsjøen disappeared by *c.* 10.1 ± 0.4 cal ka BP indicating an early onset of the glacier minimum in northern Svalbard. This is at least *c.* 1.0 ka earlier compared to most lake sediment records from the Canadian Arctic and Greenland, but *c.* 1.0 to 2.0 ka later than in the Russian archipelagos.

The response of the Åsgardfonna Ice Cap to the HTM is similar to the response of smaller glaciers and ice caps in southern Greenland that all disappeared during the HTM (Larsen et al., 2019). However, the northern Greenland ice caps and glaciers most likely persisted throughout the HTM, attributed to an Early Holocene increase in winter precipitation (due to the lack of sea ice in the Arctic Ocean) that out-balanced summer ablation (Funder et al., 2011; Larsen et al., 2019).

Compared to the unsynchronised onset of the HTM across the Circum-Arctic, the onset of the Neoglacial re-growth seemingly occurred more simultaneously. Glacial meltwater sediments reoccurred in Femmilsjøen at 3.2 ± 0.2 cal ka BP. There is some evidence that glacier re-growth and the onset of the Neoglacial in the Canadian Arctic and Greenland commenced as early as *c.* 5.0 cal ka BP, but most glaciers advanced between *c.* 3.5 to 2.5 cal ka BP (Briner et al., 2016; Larsen et al., 2019). Glaciers on Severnaya Zemlya and Franz Josef Land remained small until *c.* 5.0 and 2.4 cal ka BP, respectively (Solomina et al., 2015). This more synchronous pan-Arctic onset of the Neoglacial (compared to the onset of the HTM) might be related to the absence of large residual ice bodies and their regional influence on climate on the North American continent.

6. Conclusions

In this study we used lake records from Femmilsjøen to constrain the glacial history of NW Åsgardsfonna. We found that:

- The western end of Femmilsjøen was potentially deglaciated prior to 16.1 ± 0.3 cal ka BP, however glaciers (Åsgardfonna) persisted in the catchment area until *c.* 10.1 ± 0.4 cal ka BP.
- The lake was isolated from the marine environment due to glacioisostatic rebound between 11.7 ± 0.3 to 11.3 ± 0.2 cal ka BP. The isolation was gradual and brackish conditions possibly prevailed from *c.* 13.4 cal ka BP until the final isolation.
- Glacial meltwater supply to Femmilsjøen was absent between 10.1 ± 0.4 and 3.2 ± 0.2 cal ka BP. This period includes the Holocene Thermal Maximum. The lack of glacial meltwater runoff implies that the glaciers had effectively retreated out of the catchment, suggesting that Åsgardfonna was significantly smaller or absent from 10.1 ± 0.4 to 3.2 ± 0.2 cal ka BP.
- Minerogenic sediments reoccur in the Femmilsjøen sedimentary record from *c.* 3.2 ± 0.2 cal ka BP, implying re-growth of the glaciers in the catchment area due to Neoglacial cooling. At *c.* 2.1 ± 0.7 cal ka BP, the glaciers reached a size no smaller than their present extent.
- The Femmilsjøen catchment records Holocene variations of a larger Svalbard ice cap in a confined sedimentary basin. The record confirms Holocene glacier fluctuations observed in northern Wijdefjorden and improves the time constraints on the Holocene glacial events in the area. It serves as an important link between Svalbard data series from lacustrine archives of smaller glaciers and cirques and the larger and less confined marine fjord archives of the larger ice caps.
- Variations in the extent of Åsgardfonna during the deglaciation and the Holocene are strongly coupled to atmospheric and ocean forcings. In a Circum-Arctic perspective, this is comparable to the behaviour of glaciers and ice caps in southern Greenland and Franz Josef Land and Severnaya Zemlya.

Declaration of competing interest

The authors declare that they have no known competing financial interests or personal relationships that could have appeared to influence the work reported in this paper.

References

Aagaard, K., Foldvik, A., Hillman, S., 1987. The West Spitsbergen Current: disposition and water mass transformation. J. Geophys. Res. Oceans 92, 3778–3784.

Allaart, L., Müller, J., Schomacker, A., Rydningen, T.A., Håkansson, L., Kjellman, S.E., Mollenhauer, G., Forwick, M., 2020. Late Quaternary glacier and sea ice history of northern Wijdefjorden, Svalbard. Boreas. https://doi.org/10.1111/bor.12435.

Baeten, N.J., Forwick, M., Vogt, C., Vorren, T.O., 2010. Late Weichselian and Holocene sedimentary environments and glacial activity in Billefjorden. Svalbard. Geol. Soc. Lond. Spec. Publ. 344, 207–223.

Bakke, J., Balascio, N., van der Bilt, W.G.M., Bradley, R., D'Andrea, W.J.D., Gjerde, M., Ólafsdóttir, S., Røthe, T., de Wet, G., 2018. The Island of Amsterdamøya: a key site for studying past climate in the arctic archipelago of Svalbard. Quat. Sci. Rev. 183, 157–163.

Bartels, M., Titschack, J., Fahl, K., Stein, R., Seidenkrantz, M.-S., Hillaire-Marcel, C., Hebbeln, D., 2017. Atlantic Water advection vs. glacier dynamics in northern Spitsbergen since early deglaciation. Clim. Past 13, 1717–1749.

Bartels, M., Titschack, J., Fahl, K., Stein, R., Hebbeln, D., 2018. Wahlenbergfjord, eastern Svalbard: a glacier-surrounded fjord reflecting regional hydrographic variability during the Holocene? Boreas 47, 1003–1021.

Berger, A.L., 1978. Long-term variations of daily insolation and quaternary climatic changes. J. Atmos. Sci. 35, 2362–2367.

van der Bilt, W.G., Bakke, J., Vasskog, K., D'Andrea, W.J., Bradley, R.S., Ólafsdóttir, S.,

2015. Reconstruction of glacier variability from lake sediments reveals dynamic Holocene climate in Svalbard. Quat. Sci. Rev. 126, 201–218.

van der Bilt, W.G., D'Andrea, W.J., Werner, J.P., Bakke, J., 2019. Early Holocene temperature oscillations exceed amplitude of observed and projected warming in Svalbard lakes. Geophys. Res. Lett. 46, 14732–14741.

Batchelor, C., Dowdeswell, J., Hogan, K., 2011. Late Quaternary ice flow and sediment delivery through Hinlopen Trough, Northern Svalbard margin: submarine landforms and depositional fan. Mar. Geol. 284, 13–27.

Birks, H.H., 1991. Holocene vegetational history and climatic change in west Spitsbergen-plant macrofossils from Skardtjørna, an Arctic lake. Holocene 1, 209–218.

Blaauw, M., 2010. Methods and code for 'classical' age-modelling of radiocarbon sequences. Quat. Geochronol. 5, 512–518.

Blaauw, M., Christen, J.A., 2011. Flexible paleoclimate age-depth models using an autoregressive gammaprocess. Bayesian Anal. 6, 457–474.

Blaauw, M., Christen, J.A., Vazquez, J.E., Goring, S., 2020. Package 'clam', vol. 5, pp. 2–3. August 10.

Bradley, R.S., Mackay, A., Battarbee, R., Birks, J., Oldfield, F., 2003. Climate forcing during the Holocene. In: Global Change in the Holocene. UK Hodder Arnold, London, pp. 10–19.

Bradley, R.S., Bakke, J., 2019. Is there evidence for a 4.2 ka BP event in the northern North Atlantic region? Clim. Past 15, 1665–1676.

Braun, C., 2019. Late Weichselian and Holocene Glacier Dynamics and Sedimentary Processes in and North of the Wijdefjorden-Austfjorden Fjord System, North Spitsbergen. UiT the Arctic University of Norway, p. 111. M.Sc. thesis.

Briner, J.P., McKay, N.P., Axford, Y., Bennike, O., Bradley, R.S., de Vernal, A., Fisher, D., Francus, P., Fréchette, B., Gajewski, K., Jennings, A., Kaufman, D.S., Miller, G., Rouston, C., Wagner, B., 2016. Holocene climate change in Arctic Canada and Greenland. Quat. Sci. Rev. 147, 340–364.

Dallmann, W.K., 2015. Geoscience Atlas of Svalbard. Nor, vol. 148. Polar Institute, Report Series, p. 292.

Divine, D., Isaksson, E., Martma, T., Meijer, H.A.J., Moore, J., Pohjola, V., van der Wal, R.S.W., Godtliebsen, F., 2011. Thousand years of winter surface air temperature variations in Svalbard and northern Norway reconstructed from ice-core data. Polar Res. 30 https://doi.org/10.3402/polar.v30i0.7379.

Dunlea, A.G., Murray, R.W., Tada, R., Alvarez-Zarikian, C.A., Anderson, C.H., Gilli, A., Giosan, L., Gorgas, T., Hennekam, R., Irino, T., Murayama, M., Peterson, L.C., Reichart, G.-J., Seki, A., Zheng, H., Ziegler, M., 2020. Intercomparison of XRF core scanning results from Seven labs and approaches to practical calibration. Geochem. Geophys. Geosyst. 21, e2020GC009248.

Elverhøi, A., Lonne, O., Seland, R., 1983. Glaciomarine sedimentation in a modern fjord environment, Spitsbergen. Polar Res. 1, 127–150.

Eyles, N., Eyles, C.H., Miall, A., 1983. Lithofacies types and vertical profile models; an alternative approach to the description and environmental interpretation of glacial diamict and diamictite sequences. Sedimentology 30, 393–410.

Farnsworth, W.R., Ingolfsson, O., Noormets, R., Allaart, L., Alexanderson, H., Henriksen, M., Schomacker, A., 2017. Dynamic Holocene glacial history of St. Jonsfjorden, Svalbard. Boreas 46, 585–603.

Farnsworth, W.R., Ingolfsson, O., Retelle, M., Allaart, L., Håkansson, L.M., Schomacker, A., 2018. Svalbard glaciers re-advanced during the Pleistocene–Holocene transition. Boreas 47, 1022–1032.

Farnsworth, W.R., Ingolfsson, O., Alexanderson, H., Allaart, L., Forwick, M., Noormets, R., Retelle, M., Schomacker, A., 2020. Holocene glacial history of Svalbard - status, perspectives and challenges. Earth Sci. Rev. 208, 103249.

Fischer, H., 58 others, 2018. Palaeoclimate constraints on the impact of 2°C anthropogenic warming and beyond. Nat. Geosci. 11, 474–485.

Fjeldskaar, W., Bondevik, S., Amantov, A., 2018. Glaciers on Svalbard survived the Holocene thermal optimum. Quat. Sci. Rev. 199, 18–29.

Flink, A.E., Noormets, R., Fransner, O., Hogan, K.A., O'Regan, M., Jakobsson, M., 2017. Past ice flow in Wahlenbergfjorden and its implications for late Quaternary ice sheet dynamics in northeastern Svalbard. Quat. Sci. Rev. 163, 162–179.

Forwick, M., Vorren, T.O., 2009. Late Weichselian and Holocene sedimentary environments and ice rafting in Isfjorden, Spitsbergen. Paleogeogr. Paleoclimatol. Palaeoecol. 280, 258–274.

Forwick, M., Vorren, T.O., 2010. Stratigraphy and deglaciation of the Isfjorden area, Spitsbergen. Nor. J. Geol. 163–179.

Funder, S., Goosse, H., Jepsen, H., Kaas, E., Kjær, K.H., Korsgaard, N.J., Larsen, N.K., Linderson, H., Lyså, A., Möller, P., Olsen, J., Willerslev, E., 2011. A 10,000-year record of Arctic Ocean sea-ice variability–view from the beach. Science 333, 747–750.

Furrer, G., Stapfer, A., Glaser, U., 1991. Zur nacheiszeitlichen Gletschergeschichte des Liefdefjords (Spitzbergen)* (Ergebnisse der Geowissenschaftlichen Spitzbergenexpedition 1990). Geogr. Helv. 4, 147–155.

Fürst, J.J., 25 others., 2018. The ice-free topography of Svalbard. Geophys. Res. Lett. 45 (21), 11–76.

Gjermundsen, E.F., Briner, J.P., Akçar, N., Salvigsen, O., Kubik, P., Gantert, N., Hormes, A., 2013. Late Weichselian local ice dome configuration and chronology in Northwestern Svalbard: early thinning, late retreat. Quat. Sci. Rev. 72, 112–127. https://doi.org/10.1016/j.quascirev.2013.04.006.

Hagen, J.O., Liestøl, O., Roland, E., Jørgensen, T., 1993. Glacier Atlas of Svalbard and Jan Mayen. Nor. Polar Inst., p. 167

Hagen, J.O., Melvold, K., Pinglot, F., Dowdeswell, J.A., 2002. On the net mass balance of the glaciers and ice caps in Svalbard, Norwegian arctic. Arctic Antarct. Alpine Res. 35, 264–270.

Hald, M., Ebbesen, H., Forwick, M., Godtliebsen, F., Khomenko, L., Korsun, S., Olsen, L.R., Vorren, T.O., 2004. Holocene paleoceanography and glacial history of the West Spitsbergen area, Euro-Arctic margin. Quat. Sci. Rev. 23, 2075–2088.

Hanssen-Bauer, I., Førland, E.J., Hisdal, H., Mayer, S., Sandø, A.B., Sorteberg, A., 2019. Climate in Svalbard 2100. Norwegian Centre for Climate Services Reports. The Norwegian Centre for Climate Services (NCCS). http://bora.uib.no/handle/1956/19136.

Heaton, T.J., Köhler, P., Butzin, M., Bard, E., Reimer, R.W., Austin, W.E.N., Bronk, C.B., Grootes, P.M., Hughen, K.A., Kromer, B., Reimer, P.J., Adkins, J., Burke, A., Cook, M.S., Olsen, J., Skinner, L., 2020. Marine20-the marine radiocarbon age calibration curve (0-55,000 cal BP). Radiocarbon 62, 1–43.

Hogan, K.A., Dowdeswell, J.A., Noormets, R., Evans, J., Ó Cofaigh, C., 2010. Evidence for full-glacial flow and retreat of the late weichselian ice sheet from the waters around Kong Karls Land, eastern Svalbard. Quat. Sci. Rev. 29, 3563–3582.

Heiri, O., Lotter, A.F., Lemcke, G., 2001. Loss on ignition as a method for estimating organic and carbonate content in sediments: reproducibility and comparability of results. J. Paleolimnol. 25, 101–110.

Hogan, K.A., Dowdeswell, J.A., Hillenbrand, C.D., Ehrmann, W., Noormets, R., Wacker, L., 2017. Subglacial sediment pathways and deglacial chronology of the northern Barents Sea Ice Sheet. Boreas 46, 750–771.

Holm, T.M., Koinig, K.A., Andersen, T., Donali, E., Hormes, A., Klaveness, D., Psenner, R., 2012. Rapid physicochemical changes in the high Arctic Lake Kongressvatn caused by recent climate change. Aquat. Sci. 74, 385–395. https://doi.org/10.1007/s00027-011-0229-0.

Hormes, A., Gjermundsen, E.F., Rasmussen, T.L., 2013. From mountain top to the deep sea — deglaciation in 4D of the northwestern Barents Sea ice sheet. Quat. Sci. Rev. 75, 78–99.

Howe, J.A., Shimmield, T.M., Harland, R., 2008. Late quaternary contourites and glaciomarine sedimentation in the Fram Strait. Sedimentology 55, 179–200.

Hughes, A.L.C., Gyllencreutz, R., Lohne, Ø.S., Mangerud, J., Svendsen, J.I., 2016. The last Eurasian ice sheets—a chronological database and time-slice reconstruction. DATED-1. Boreas 45, 1–45.

Isaksson, E., Kohler, J., Pohjola, V., Moore, J., Igarashi, M., Karlöf, L., Martma, T., Meijer, H., Motoyama, H., Vaikmäe, R., van de Wal, R.S.W., 2005. Two ice-core δ¹⁸O records from Svalbard illustrating climate and sea-ice variability over the last 400 years. Holocene 15, 501–509.

Joo, Y.J., Forwick, M., Park, K., Joe, Y., Son, Y.J., Nam, S., 2019. Holocene environmental changes in Dicksonfjorden, West Spitsbergen, Svalbard. Polar Res. 38, 3426.

Kaufman, D.S., Ager, T.A., Anderson, N.J., Anderson, P.M., Andrews, P.M., Bartlein, P.J., Brubaker, L.B., Coats, L.L., Cwynar, L.C., Duvall, M.L., Dyke, A.S., Edwards, M.E., Eisner, W.R., Gajewski, K., Geirsdóttir, A., Hu, F.S., Jennings, A., Kaplan, M.R., Kerwin, M.W., Lozhkin, A.V., MacDonald, G.M., Miller, G.H., Mock, C.J., Oswald, W.W., Otto-Bliesner, B.L., Porinchu, D.F., Rühland, K., Smol, J.P., Steig, E.J., Wolfe, B.B., 2004. Holocene thermal maximum in the western Arctic (0–180°W). Quat. Sci. Rev. 23, 529–560.

Karlén, W., Matthews, J.A., 1992. Reconstructing Holocene glacier variations from glacial lake sediments: studies from nordvestlandet and Jostedalsbreen-Jotunheimen, southern Norway. Geogr. Ann. 74, 327–348.

Kekonen, T., Moore, J., Perämäki, P., Mulvaney, R., Isaksson, E., Pohjola, V., van de Wal, R.S.W., 2005. The 800 year long ion record from the Lomonosovfonna (Svalbard) ice core. J. Geophys. Res. 110, D07304. https://doi.org/10.1029/2004JD005223.

Kjellman, S.E., Schomacker, A., Thomas, E.K., Håkansson, L., Duboscq, S., Cluett, A.A., Farnsworth, W.R., Allaart, L., Cowling, O.C., McKay, N.P., Brynjólfsson, S., Ingolfsson, O., 2020. Holocene precipitation seasonality in northern Svalbard: influence of sea ice and regional ocean surface conditions. Quat. Sci. Rev. 240, 1–15. https://doi.org/10.1016/j.quascirev.2020.106388, 106388.

Koc, N., Klitgaard-Kristensen, D., Hasle, K., Forsberg, C.F., Solheim, A., 2002. Late glacial palaeoceanography of Hinlopen strait, northern Svalbard. Polar Res. 21, 307–314.

Krüger, J., Kjær, K.H., 1999. A data chart for field description and genetic interpretation of glacial diamicts and associated sediments — with examples from Greenland, Iceland and Denmark. Boreas 28, 386–402.

Kylander, M.E., Ampel, L., Wohlfarth, B., Veres, D., 2011. High-resolution X-ray fluorescence core scanning analysis of Les Echets (France) sedimentary sequence: new insights from chemical proxies. J. Quat. Sci. 26, 109–117.

Larsen, E.A., Lyså, A., Rubensdotter, L., Farnsworth, W.R., Jensen, M., Nadeau, M.J., Ottesen, D., 2018. Late-glacial and Holocene glacier activity in the van Mijenfjorden area, western Svalbard. Arktos 4, 9. https://doi.org/10.1007/s41063-018-0042-2.

Larsen, N.K., Strunk, A., Levy, L.B., Olsen, J., Bjørk, A., Lauridsen, T.L., Jeppesen, E., Davidson, T.A., 2017. Strong altitudinal control on the response of local glaciers to Holocene climate change in southwest Greenland. Quat. Sci. Rev. 168, 69–78.

Larsen, N.K., Strunk, A., Levy, A., Søndergaard, A.S., Olsen, J., Lauridsen, T.L., 2019. Local ice caps in finderup Land, north Greenland, survived the Holocene thermal maximum. Boreas 48, 551–562.

Laskar, J., Robutel, P., Joutel, F., Gastineau, M., Correia, A., Levrard, B., 2004. A long-term numerical solution for the insolation quantities of the Earth. Astron. Astrophys. 428, 261–285.

Landvik, J.Y., Brook, E.J., Gualtieri, L., Raisbeck, G., Salvigsen, O., Yiou, F., 2003. Northwest Svalbard during the last glaciation: ice-free areas existed. Geology 31, 906–908.

Licht, K.J., Cunningham, W.L., Andrews, J.T., Domack, E.W., Jennings, A.E., 1998. Establishing chronologies from acid-insoluble organic ¹⁴C dates on antarctic (Ross Sea) and arctic (North Atlantic) marine sediments. Polar Res. 17, 203–216.

Liestøl, O., 1993. The Glaciers of Svalbard, Norway. U.S. Geo. Sur, pp. 127–151.

Professional Paper 1386-E.

Lowe, J., Walker, M. (Eds.), 2015. Reconstructing Quaternary Environments, third ed. Routledge, London, pp. 151—165.

Lønne, I., 2005. Faint traces of high Arctic glaciations: an early Holocene ice-front fluctuation in Bolterdalen, Svalbard. Boreas 34, 308—323.

Lønne, I., 2016. A new concept for glacial geological investigations of surges, based on High-Arctic examples (Svalbard). Quat. Sci. Rev. 132, 74—100.

Mangerud, J., Bolstad, M., Elgersma, A., Helliksen, D., Landvik, J.Y., Lønne, I., Lycke, A.K., Salvigsen, O., Sandahl, T., Svendsen, J.I., 1992. The last glacial maximum on Spitsbergen. Quat. Res. 38, 1—31.

Mangerud, J., Bondevik, S., Gulliksen, S., Hufthammer, A.K., Høisæter, T., 2006. Marine 14C reservoir ages for 19th century whales and molluscs from the North Atlantic. Quat. Sci. Rev. 25, 3228—3245.

Mangerud, J., Svendsen, J.I., 2018. The Holocene thermal optimum around Svalbard, Arctic North Atlantic; molluscs show early and exceptional warmth. Holocene 28, 65—83.

Marlin, C., Tolle, F., Griselin, M., Bernard, E., Saintenoy, A., Quenet, M., Friedt, J.-M., 2017. Change in geometry of a high arctic glacier from 1948 to 2013 (Austre Lovénbreen, Svalbard). Geogr. Ann. Ser. A Phys. Geogr. 115—138.

Martin-Puertas, C., Tjallingii, R., Bloemsma, M., Brauer, A., 2017. Varved sediment responses to early Holocene climate and environmental changes in Lake Meerfelder Maar (Germany) obtained from multivariate analyses of micro X-ray fluorescence core scanning data. J. Quat. Sci. 32, 427—436.

Miller, G.H., Landvik, J.Y., Lehman, S.J., Southon, J.R., 2017. Episodic Neoglacial snowline descent and glacier expansion on Svalbard reconstructed from the 14C ages of ice-entombed plants. Quat. Sci. Rev. 155, 67—78.

Mäusbacher, R., Borg, K.V.D., Daut, G., Kroemer, E., Müller, J., Wallner, J., 2002. Late Pleistocene and Holocene environmental changes in NW Spitsbergen — evidence from lake sediments. Z. Geomorphol. 46, 417—439.

Norwegian Polar Institute, 2019. TopoSvalbard, Topographic Map over Svalbard accessed on. https://toposvalbard.npolar.no/. (Accessed 10 November 2019).

Polyak, L., Solheim, A., 1994. Late- and postglacial environments in the northern Barents Sea west of Franz Josef Land. Polar Res. 13, 197—207.

R Core Team, 2020. R: A Language and Environment for Statistical Computing. R Foundation for Statistical Computing, Vienna, Austria. Retrieved from. https://www.R-project.org/.

Rasmussen, T.L., Forwick, M., Mackensen, A., 2013. Reconstruction of inflow of Atlantic water to Isfjorden, Svalbard during the Holocene: correlation to climate and seasonality. Mar. Micropaleontol. 99, 18—28.

Reimer, P.J., Austin, W.E.N., Bard, E., Bayliss, A., Blackwell, P.G., Ramsey, C.B., Butzin, M., Cheng, H., Edwards, R.L., Friedrich, M., Grootes, P.M., Guilderson, T.P., Hajdas, I., Heaton, T.J., Hogg, A.G., Hughen, K., Kromer, B., Manning, S.W., Muscheler, R.J., Palmer, G., Pearson, C., van der Plicht, J., Reimer, R.W., Richards, D.A., Scott, E.M., Southon, J.R., Turney, C.S.M., Wacker, L., Adolphi, F., Büntgen, U., Capano, M., Fahrni, S., Fogtmann-Schulz, A., Friedrich, R., Miyake, F., Olsen, J., Reinig, F., Sakamoto, M., Sookdeo, A., Talamo, S., 2020. The IntCal20 northern hemisphere radiocarbon age calibration curve (0-55 cal kBP). Radiocarbon 62, 725—757.

Røthe, T.O., Bakke, J., Vasskog, K., Gjerde, M., D'Andrea, W.J., Bradley, R.S., 2015. Arctic Holocene glacier fluctuations reconstructed from lake sediments at Mitrahalvøya, Spitsbergen. Quat. Sci. Rev. 109, 111—125.

Røthe, T.O., Bakke, J., Støren, E.W., Bradley, R.S., 2018. Reconstructing Holocene glacier and climate fluctuations from lake sediments in Vårfluesjøen, northern Spitsbergen. Front. Earth Sci. 6, 1—20.

Salvigsen, O., Österholm, H., 1982. Radiocarbon dated raised beaches and glacial history of the northern coast of Spitsbergen, Svalbard. Polar Res. 1, 97—115.

Salvigsen, O., Forman, S.L., Miller, G.H., 1992. Thermophilous molluscs on Svalbard

during the Holocene and their paleoclimatic implications. Polar Res. 11, 1—10.

Schildgen, T., Dethier, D.P., Bierman, P., Caffee, M., 2002. 26Al and 10Be dating of late pleistocene and Holocene fill terraces: a record of fluvial deposition and incision, Colorado front range. Earth Surf. Process. Landforms 27, 773—787.

Schnurrenberger, D., Russell, J., Kelts, K., 2003. Classification of lacustrine sediments based on sedimentary components. J. Paleolimnol. 29, 141—154.

Schomacker, A., Farnsworth, W.R., Ingolfsson, O., Allaart, L., Håkansson, L., Retelle, M., Siggaard-Andersen, M.-L., Korsgaard, N.J., Rouillard, A., Kjellman, S.E., 2019. Postglacial relative sea level change and glacier activity in the early and late Holocene: Wahlenbergfjorden, Nordaustlandet, Svalbard. Sci. Rep. 9, 1—13, 6799.

Ślubowska, M.A., Koç, N., Rasmussen, T.L., Klitgaard-Kristensen, D., 2005. Changes in the flow of Atlantic water into the Arctic Ocean since the last deglaciation: Evidence from the northern Svalbard continental margin 80°N. Paleoceanogr. Paleoclim. https://doi.org/10.1029/2005PA001141.

Smith, N.D., Ashley, G., 1985. Proglacial lacustrine environment. In: Glacial Sedimentary Environments. SEPM Short Course, vol. 16, pp. 135—216.

Svendsen, J.I., Landvik, J.Y., Mangerud, J., Miller, G.H., 1987. Postglacial marine and lacustrine sediments in Linnévatnet, Svalbard. Polar Res. 5, 281—283.

Svendsen, J.I., Mangerud, J., Miller, G., 1989. Denudation rates in the Arctic estimated from lake sediments on Spitsbergen, Svalbard. Palaeogeogr. Palaeoclimatol. Palaeoecol. 76, 153—168.

Svendsen, J.I., Mangerud, J., Elverhøi, A., Solheim, A., Schüttenhelm, R.T.E., 1992. The Late Weichselian glacial maximum on western Spitsbergen inferred from offshore sediment cores. Mar. Geol. 104, 1—17.

Svendsen, J.I., Mangerud, J., 1997. Holocene glacial and climatic variations on Spitsbergen, Svalbard. Holocene 7, 45—57.

Snyder, J., Miller, G., Werner, A., Jull, A., Stafford, T., 1994. AMS-radiocarbon dating of organic-poor lake sediment, an example from Linnévatnet, Spitsbergen, Svalbard. Holocene 4, 413—421.

Snyder, J.A., Werner, A., Miller, G.H., 2000. Holocene Cirque Glacial Activity in Western Spitsbergen, Svalbard: Sediment Records from Proglacial Linnévatnet. The Holocene 10, pp. 555—563.

Solomina, O.N., Bradley, R.S., Hodgson, D.A., Ivy-Ochs, S., Jomelli, V., Mackintosh, A.N., Nesje, A., Owen, L.A., Wanner, H., Wiles, G.C., Young, N.E., 2015. Holocene glacier fluctuations. Quat. Sci. Rev. 111, 9—34.

Trottier, A., Lajeunesse, P., Gagnon-Poiré, A., Francus, P., 2019. Morphological signatures of deglaciation and postglacial sedimentary processes in a deep fjord-lake (Grand Lake, Labrador). Earth Surf. Process. Landforms 45, 928—947.

Voldstad, L.H., Alsos, I.G., Farnsworth, W.R., Heintzman, P.D., Håkansson, L., Kjellman, S.E., Rouillard, A., Schomacker, A., Eidesen, P.B., 2020. A complete Holocene lake sediment ancient DNA record reveals long-standing high Arctic plant diversity hotspot in northern Svalbard. Quat. Sci. Rev. 234, 1—15, 106207.

Walker, M., 2005. Radiometric dating 1: radiocarbon dating. In: Quaternary Dating Methods. John Wiley & Sons Inc, New York, pp. 17—55.

Weltje, G.J., Tjallingii, R.J.E., Letters, P.S., 2008. Calibration of XRF core scanners for quantitative geochemical logging of sediment cores: theory and application. Earth Planet Sci. Lett. 274, 423—438.

Werner, K., Müller, J., Husum, K., Spielhagen, R.F., Kandiano, E.S., Polyak, L., 2016. Holocene sea subsurface and surface water masses in the Fram Strait—Comparisons of temperature and sea-ice reconstructions. Quat. Sci. Rev. 147, 194—209. https://doi.org/10.1016/j.quascirev.2015.09.007.

de Wet, G.A., Balascio, N., D'Andrea, W.J., Bakke, J., Bradley, R.S., Perren, B., 2018. Holocene glacier activity reconstructed from proglacial lake Gjøavatnet on Amsterdamøya, NW Svalbard. Quat. Sci. Rev. 183, 188—203.

X-Rite, 2015. The Munsell Soil Color Book (M50215B). 2009 Revised Edition, 2015 production.